~~Influence~~ Modulation of tropical stratospheric gravity wave activity and ITCZ position by modes of climate variability ~~on stratospheric gravity waves~~ in ~~the tropics using Radio Occultation~~ radio occultations and ~~Reanalysis Data~~reanalyses

Toyese Tunde Ayorinde[1], Cristiano Max Wrasse[1], Hisao Takahashi[1], Luiz Fernando Sapucci[2], Mohamadou A. Diallo[3], Cosme Alexandre Oliveira Barros Figueiredo[4], Diego Barros[1], Ligia Alves da Silva[1], Patrick Essien[5], and Anderson Vestena Bilibio[4]

[1]Space Weather Division, National Institute for Space Research (INPE), São José dos Campos, SP, Brazil
[2]Instituto Nacional de Pesquisas Espaciais (INPE), Centro de Previsão de Tempo e Estudos Climáticos, Rodovia Presidente Dutra, km 40, Cachoeira Paulista, SP, Brazil
[3]Institute of Climate and Energy Systems – Stratosphere (ICE-4), Forschungszentrum Jülich GmbH, 52428 Juelich, Germany, m.diallo@fz-juelich.de
[4]Unidade Acadêmica de Física, Universidade Federal de Campina Grande, Campina Grande, PB, Brazil
[5]University of Cape Coast, Department of Physics, Meteorology and Atmospheric Research Lab, Cape Coast, Ghana, patrick.essien@ucc.edu.gh

Correspondence: Toyese Tunde Ayorinde (toyese.ayorinde@inpe.br)

Abstract. The Intertropical Convergence Zone (ITCZ) is a ~~critical driver~~ dominant feature of tropical climate ~~, characterized by convective activity that transfers energy, influences atmospheric circulation, and modulates precipitation. These processes generate atmospheric disturbances, making the ITCZ a significant~~ characterized by intense convection that influences global atmospheric circulation and serves as a primary source of stratospheric gravity waves (GWs), which transport energy and momentum vertically through the atmosphere. This study investigates the ~~relationship between the ITCZand stratospheric GWs, as well as the influence of climate variability modes—Madden-Julian Oscillation (MJO), El Niño–Southern Oscillation (ENSO), and Quasi-Biennial Oscillation (QBO)—on GW activity and ITCZ dynamics. Using GNSS radio occultation (RO) data from COSMIC-1~~modulation of tropical Intertropical Convergence Zone (ITCZ) position and stratospheric gravity wave activity by ENSO, MJO, ~~COSMIC-2, and METOP satellites (2011–2021) , we derive the latitudinal positions of the ITCZ and GW potential energy (Ep) maxima~~ and QBO using 11 years (2011-2021) of radio occultation and reanalysis data. ITCZ latitude (from 850 hPa refractivity) and gravity wave potential energy maxima (from stratospheric temperatures) were identified via Gaussian fitting. ~~ERA5 and NCEP reanalysis data are used to validate ITCZ positions and estimate refractivity. Results show the ITCZ migrates~~ Both ITCZ and gravity wave potential energy maxima exhibit coherent seasonal migration ($\sim$10° ~~latitudinally, with~~ and $\sim$5° ~~seasonal shifts between boreal winter and summer, while its strength remains relatively stable. Stratospheric GW Ep maxima exhibit seasonal patterns similar to the ITCZ, with smaller latitudinal gaps in the Northern and Southern Hemispheres. Multilinear regression reveals significant zonal variations in the impacts of QBO, ENSO , and MJO on ITCZ position and Ep, particularly over the American , African, and Asian sectors~~latitudinal shifts respectively), with potential

energy maxima typically equatorward of the ITCZ. ~~ENSO and MJO drive substantial negative trends in ITCZposition, Ep, and refractivity, especially in Asian and Africanregions. However, zonal trends in Ep maxima and ITCZ positions remain stable, likely due to consistent Gaussian peak locations. Discrepancies in ITCZtrends and refractivity valuesbetween RO, ERA5, and NCEP data are attributed to differences in resolution, coverage, and assimilation techniques. This study highlights the complex interplay between the ITCZ, GWs, and climate variability modes~~ENSO is the primary modulator: El Niño conditions shift ITCZ northward in the American sector but southward in African/Asian sectors; for gravity wave potential energy maxima, El Niño induces southward shifts in the American sector but northward shifts in the Asian sector, while enhancing overall GW activity. MJO prompts regionally complex southward shifts of ITCZ/potential energy maxima. QBO predominantly influences gravity wave potential energy, with westerly phases linked to southward shifts of potential energy maxima in African/Asian sectors. While long-term latitudinal trends are weak, climate modes significantly impact ITCZ/GW peak values. The radio occultation data captured finer-scale features than reanalysis products, highlighting the importance of observational constraints in understanding troposphere-stratosphere coupling mechanisms.

1 Introduction

The tropical atmosphere is ~~a complex system involving dynamic interactions between different atmospheric modes of climate variability that modify~~ characterized by complex interactions between convective processes, large-scale circulation patterns, and wave dynamics that collectively influence global weather and climate~~on various temporal and spatial scales. These modes of climate variability include the Madden-Julian Oscillation (MJO), the El Niño-Southern Oscillation (ENSO), and the Quasi-Biennial Oscillation (QBO), which have a highly effective influence on the variability of~~ . At the heart of this system lies the Intertropical Convergence Zone (ITCZ)~~(???). QBO, ENSO, and MJO not only imply changes in the weather at the surface but also play an important role in the dynamics of the upper atmosphere, influencing the generation of convective~~ , a narrow band of intense convection and precipitation that forms where the northeast and southeast trade winds converge near the equator (?). The ITCZ not only serves as a key component of the global circulation system but also acts as a significant source of atmospheric gravity waves (~~GWs) in the equatorial stratosphere and their upward propagation. GWs play a vital role in improving the accuracy of climate model simulations, particularly in representing modes of climate variability. This is due to their interaction with sea surface temperature anomalies associated with key modes of variability, such as the~~ GW) that transport energy and momentum vertically through the atmosphere (?????).

GWs are small-scale atmospheric oscillations that play a crucial role in connecting different atmospheric layers (??). In the tropics, these waves, mainly generated by deep convection and flow over topography (???), propagate into the stratosphere and beyond, influencing circulation patterns such as Brewer-Dobson circulation and Quasi-Biennial Oscillation (QBO) (??). The potential energy (Ep) of these waves serves as a valuable proxy for GW activity (??).

Three major modes of climate variability significantly influence the tropical atmosphere: the Madden-Julian Oscillation (MJO), ~~El Niño-Southern~~ the El Niño-Southern Oscillation (ENSO), and ~~Quasi-Biennial Oscillation (QBO). A good representation of the QBO, for example, is essential for the quality of these simulations.~~

The ITCZ is a near-equatorial zone of convergence of the Northern and Southern Hemisphere trade winds characterized by convective activity and is an essential source of the GWs. Variability, location, and strength of the ITCZ are affected by the already mentioned modes of climate variability (??). The evidence of convective activity propagating along the intermediate axis of the eastern Pacific ITCZ has been studied using the characteristics of Kelvin waves, including its spatial structure propagation rate and characteristics of Kelvin waves (?). ? studied the dynamics of GWs associated with convection propagating through a precipitation region analyzed in an idealized model of the large-scale atmospheric circulationQBO. These modes modulate both the position and intensity of the ITCZ (?????) and affect the generation and propagation of stratospheric GWs through various mechanisms. Characterized by eastward propagating convective anomalies with a 30-90-day periodicity, the MJO can enhance GW activity through increased convection (?????). ENSO alters Walker circulation (an east-west atmospheric circulation along the equator, with rising air over the warm western Pacific and sinking air over the cooler eastern Pacific) and shifts the regions of maximum convection in the tropical Pacific (?), affecting GW generation and propagation through changes in background winds and temperatures (????). With its alternating easterly and westerly wind regimes in the equatorial stratosphere, the QBO directly influences the vertical propagation of GWs through critical-level filtering and wave-mean flow interactions (????). Recent research has also revealed a relationship between QBO and MJO amplitude during boreal winter (?), further highlighting the interconnected nature of these climate modes.

The ITCZ position varies seasonally, typically following the region of maximum solar heating with a delay of 1-2 months, moving north during boreal summer and south during boreal winter (??). Several methods have been developed to determine the ITCZ(?), including determining the location of maximum precipitation above a certain threshold, using visible and infrared satellite observations of highly reflective cloud cover, estimating wind field convergence identify and track ITCZ, assessing relative vorticity structures, and using multiple variable criteria (?). ? determined the ITCZ using specific humidity from two European Centre for Medium-Range Weather Forecasts (ECMWF) reanalyses dataset. In addition, ? determined the ITCZ using 13 years of refraction data from including those based on precipitation maxima (?), outgoing long-wave radiation (OLR) minima (??), surface wind convergence (?), and specific humidity distributions (?). More recently, ? demonstrated that atmospheric refractivity derived from measurements of radio occultation (RO) of the Global Navigation Satellite System (GNSS) radio occultation (RO). Detecting the ITCZis essential for various reasons (?), including its role in the emergence of equatorial stratospheric GWs.

The equatorial stratospheric GWs are a significant component of the atmospheric system and a crucial driving mechanism in the lower and middle atmospheres through drag and diffusion processes. Deep convection and flow over topography are the two most common causes of equatorial stratospheric GWs (??????). Deep convective activities are the most likely source of equatorial stratospheric GWs in the Earth's tropical zone. Studies have linked deep convection processes to the origin of GWs. The ITCZ's increased convection, cloud formation, and rainfall lead to notable changes in heat flux, moisture, and momentum within and outside its boundaries, influencing tropical circulation. These physical characteristics are essential features in generating GWs in the equatorial region. While several studies have been conducted on GWs in provides an effective means to locate the ITCZ. RO is a limb-sounding technique that provides high vertical resolution profiles of atmospheric parameters with global coverage and all-weather capability (??). The technique measures the bending of the GNSS signals as they pass through

the atmosphere, from which vertical profiles of refractivity can be derived. In the lower troposphere, refractivity is primarily sensitive to water vapour, making it an excellent tracer for moisture-related features such as ITCZ. In the stratosphere, ~~there is a lack of studies that specifically consider the link between atmospheric refractivity and equatorial stratospheric GWs. The latter plays a vital role in the upward transport of energy and momentum within the atmosphere, affecting processes like the stratosphere's circulation and the QBO. Understanding the relationship between atmospheric oscillations such as the QBO, MJO, ENSO, and stratospheric GWs is essential to understanding tropical atmospheric dynamics better. The ITCZ interacts with phenomena such as the circulation of the monsoon and the ENSO (?). There are several ways to identify the ITCZ region: the high precipitation, visible and infrared satellite observations, wind field convergence pattern, relative vorticity structures, etc.~~ temperature profiles derived from RO measurements can be used to study GW activity through the calculation of potential energy (??).

~~The interactions of different modes of climate variability~~ Although numerous studies have examined the relationship between tropical convection and stratospheric GW activity (??) and the influence of climate modes on GW (?????), fewer have explicitly linked the detailed structure and variability of ITCZ with stratospheric GW activity and their joint modulation by climate modes. This study addresses this gap by using RO data from the first and second Constellation Observing System for Meteorology, Ionosphere and Climate (COSMIC-1 and COSMIC-2), and Meteorological Operational Satellite (MetOp) satellites, along with ERA5 and NCEP reanalysis data, to investigate the relationship between ITCZ and stratospheric GW, as well as the influence of climate variability modes on both phenomena. The objectives of our study are aimed at addressing the following: (1) How do the positions of the ITCZ and stratospheric GW Ep maxima vary seasonally and interannually between different geographical regions? (2) What is the spatial relationship between the ITCZ and stratospheric GW activity in the tropics? (3) How do climate variability modes (MJO, ENSO, and QBO) ~~with refractivity and GWs are critical in understanding global atmospheric dynamics. These modes of climate variability modulate the atmospheric circulation (including background wind and temperatures), influencing GW propagation across different air layers. The MJO, for example, affects tropical convection and can boost GW activity(?). Depending on ENSO phases,~~ modulate the ~~wave-mean flow interaction differs. El Nino is associated with more wave breaking in the lower stratosphere, strengthening circulation. In contrast, La Nina is associated with a reduced wave forcing, in particular convective gravity, due partly to the reduced convective activity and change in background wind (??). The alternating wind easterly and westerly QBO affect the vertical propagation of GWs, which are critical for generating stratospheric circulation patterns (??). Understanding these interactions is essential in developing climate models and better constraining forecasting weather models since they contribute to the intricate linkage between the troposphere and stratosphere. The equatorial stratospheric GWsplay significant roles in the vertical transport of energy and momentum, significantly affecting weather and climate. There are several studies conducted on the influence of atmospheric oscillations on GWs, for example, MJO(????), ENSO(???)~~ITCZ position and stratospheric GW activity, and (4) Are there regional differences in how these climate modes influence the ITCZ and stratospheric GWs? To address these questions, we employ a Gaussian fitting method to identify the latitudinal positions of the ITCZ and GW Ep maxima, and use multilinear regression to analyze the effects of MJO, ENSO, and QBO ~~(?????), etc. ? found a strong relationship between the QBO of equatorial stratospheric winds and the amplitude of the MJO during the boreal winter has recently been uncovered~~

using observational dataon these parameters. Our approach allows us to quantify the specific contributions of each climate mode to the variability of the ITCZ and GW Ep characteristics.

This study uses RO data The paper is organized as follows. Section 2 describes the data sources and methodology, including the calculation of atmospheric refractivity, ERA5, and NCEP reanalysis data first to identify the ITCZ and the GW potential energy (E_p) maxima using the refractivityand temperature data, as well as to investigate the effects of modes of climate variability on stratospheric GWs within the ITCZ . The second goal is to understand how QBO, MJO, and ENSO modulate GWs within the ITCZ. Gravity wave studies require high-resolution RO vertical profiles of temperature, pressure, GW Ep, the identification of the ITCZ and humidity. Reanalysis products combine observations with model outputs, comprehensively describing atmospheric conditions over time. We organized the rest of this study as follows: The data subsection 2.1 describes the data. The methodology subsection 2.2 and ?? explains the methods for ITCZ identification and GW Ep. The results ?? illustrates the seasonal changes in GW, its distribution, and possible links between equatorial stratospheric GW and the ITCZ. We also discuss in ?? how ENSO, MJO, and QBO affect atmospheric refractivity and GW Ep. The conclusion in ?? provide the final remarks. Ep maxima, and the regression analysis approach. Section 3 presents the results, focusing on climatology, seasonal and interannual variations, and modulation by climate modes. Section 4 discusses the physical interpretation of the findings and compares them with previous work. Finally, Section 5 summarizes the key conclusions and suggests directions for future research.

2 Data and Methodology

2.1 Data Sources

The data used for this study is the reprocessed data set of

This study utilizes reprocessed dry temperature profiles from the satellite measurements of COSMIC -1, COSMIC -2, and METOPCOSMIC-1 and COSMIC-2, which are satellite missions that use RO to provide high-precision atmospheric data, and MetOp (a, b, c) (hereafter RO)satellite measurements (hereafter collectively referred to as RO data) for the period January 2011 to December 2021. The COSMIC-1 was launched in 2006 with six microsatellites providing approximately 1500 RO events per day. The COSMIC-2 GNSS RO observation generates approximately 5000 to 7000 RO events daily, offering ample opportunities to analyze global atmospheric variations system generates approximately 5,000 to 7,000 RO events per day, providing extensive global coverage for atmospheric analysis with high precision and accuracy. The COSMIC-2 mission generates various atmospheric parameters, such as the dry atmospheric temperature profile (atmPrf) , wet atmospheric temperature profile (wetPrf) etc. vertical resolution. The MetOp (a, b, c) are European polar-orbiting weather satellites operated by the European Organization for the Exploitation of Meteorological Satellites. Launched in 2006, 2012, and 2018 respectively, they provide high-resolution data for weather forecasting, climate monitoring, and atmospheric research.

The atmospheric profile "atmPrf" data (atmPrf) at level 2 of the COSMIC-2 data is RO dataset are processed operationally in near-real-time (nrt) without moisture information. Each atmPrf file includes contains high-resolution profiles of physical parameters like including dry pressure, dry temperature, refractivity, bending angle, impact parameters, and geometric height

above mean sea level. ~~The RO data from RO~~ All RO data were retrieved from the COSMIC Data Analysis and Archive Center (CDAAC) website ~~, which can be found at~~ (http://cdaac-www.cosmic.ucar.edu/cdaac/products.html~~. The RO data used for this study are from January 2011 and December 2021. The corresponding statistics of the available profile data used in this study are shown in .~~).

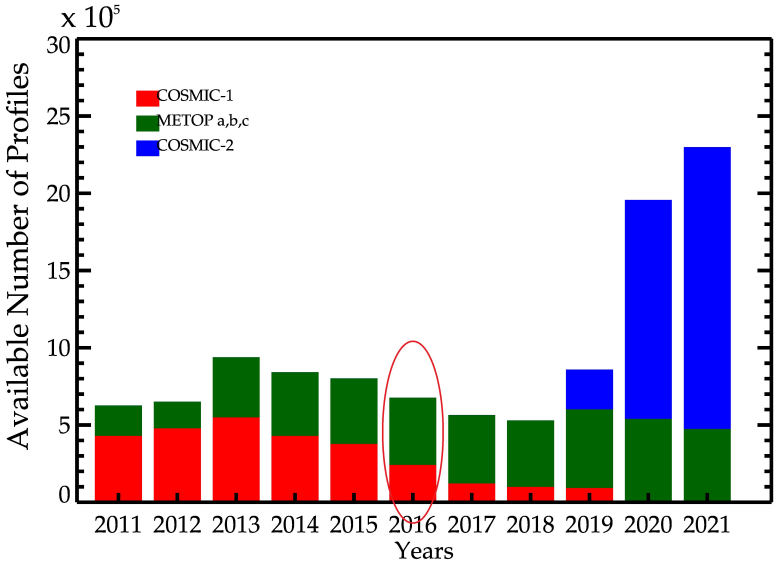

Figure 1. ~~The yearly~~ Annual statistics of available COSMIC-1, COSMIC-2, ~~the~~ and METOP temperature ~~,~~ and ~~the~~ refractivity profiles ~~for~~ between 2011 and 2021. ~~The~~ COSMIC-1 profiles are shown in red, ~~all~~ METOP profiles ~~are~~ in green, and ~~the~~ COSMIC-2 profiles ~~are~~ in blue. The ~~randomly selected temperature and refractivity~~ profiles ~~(~~highlighted in the red oval ~~)~~ were ~~used~~ randomly selected for generating example analyses in ~~that year to generate~~ Fig. 2.

~~The total numbers of temperature ("atmPrf"~~Figure 1 presents the total number of temperature profiles (atmPrf) and refractivity ~~data ("wetPrf") profiles per year are presented in~~ profiles (wetPrf) per year used in this study. The number of profiles ~~per year~~ exceeded 2 million in 2020 and 2021, ~~attributed~~ primarily due to the launch of COSMIC-2 in June 2019, ~~resulting~~ which resulted in a daily average of ~~over 5000 profiles. Temperature and relative humidity were obtained from~~ more than 5000 profiles. The RO data have a vertical resolution of approximately 100 m in the lower troposphere to about 1 km in the stratosphere, with an accuracy of 0.1-0.2 K for temperature measurements in the upper troposphere and lower stratosphere (**?**) .

To validate and complement the RO data, we also used temperature and relative humidity data from two reanalysis products:

1. ECMWF Reanalysis v5 (ERA5) (https://www.ecmwf.int/en/forecasts/dataset/ecmwf-reanalysis-v5)~~. The~~ : ERA5 is the ~~most recent climate reanalysis conducted by the ECMWF. It integrates prior data and simulations to provide a consistent time series of numerous climatic variables. ERA5 includes~~ latest climate reanalysis produced by ECMWF, providing hourly data on ~~various~~ atmospheric, land-surface, and sea-state ~~factors and~~ parameters with uncertainty estimates. ~~ERA5 uses standard~~ It uses

a latitude-longitude ~~grids~~ grid with a spatial resolution of $0.25° \times 0.25°$ ~~. The reanalysis contains data on air temperature, wind, rainfall, sea surface temperature, ocean wave height, and~~ and 137 vertical levels from the surface to 0.01 hPa. For this study, we used data on the 37 ~~pressure levels. ERA5 has been accessible since 1940 and continues to be extended ahead in time (?). Also, temperature and relative humidity were obtained from~~ standard pressure levels available in the public dataset (?).

2. Reanalysis data of the National Centers for Environmental Prediction/National Center for Atmospheric Research (NCEP/NCAR) Reanalysis data (https://psl.noaa.gov/data/reanalysis/reanalysis.shtml)~~to estimate the atmospheric refractivity from a different source. The NCEP/NCAR Reanalysis is a comprehensive dataset that~~ : This dataset combines historical observations ~~and numerical weather model simulations to provide reliable climate records. It gives 6-hourly~~ with numerical simulations of weather models to provide six-hourly and daily data from January 1948 to the present~~, including information on several atmospheric characteristics such as air temperature, wind, and precipitation (?). The~~ . It has a spatial resolution of $2.5° \times 2.5°$ with 17 pressure levels (?).

Furthermore, specific humidity, ~~outgoing long-wave radiation (OLR)~~OLR, and vertical velocity data were obtained from the NOAA ~~'s (National Oceanic and Atmospheric Administration) physical sciences laboratory~~ Physical Sciences Laboratory website (https://psl.noaa.gov/data/gridded/data.ncep.reanalysis.html) to provide context for ITCZ identification.

2.2 ~~The atmospheric refractivity~~Atmospheric Refractivity as ITCZ Proxy

~~The atmospheric~~ Atmospheric refractivity (N) in a neutral atmosphere is ~~a dimensionless quantity defined as $N = (n - 1) \times 10^6$~~defined as $N = (n - 1) \times 10^6$, where n ~~(unit less) is the atmospheric~~ is the refractive index. ~~N is given by the following and is primarily determined by water vapour and temperature gradients in the lower atmosphere:~~

It depends on pressure (P, hPa), temperature (T, K), and water vapour pressure (e, hPa) (?):

$$(N - units), \frac{e}{T^2} \tag{1}$$

where $P_d = P - e$ is the partial pressure of dry air and k_1, k_2, k_3 are constants. The simplified form on the right is commonly used, combining dry and wet terms. In the lower troposphere (e.g., 850 hPa), the wet term involving e dominates the variability of N, making refractivity a good proxy for moisture content and thus convective activity associated with ITCZ (?). We used N derived directly from RO 'wetPrf' profiles at 850 hPa. For ERA5 and NCEP, we calculate N at 850 hPa using their respective temperature, pressure (implicitly through the 850 hPa level) and humidity data via Eq. (1). Using refractivity allows for a consistent proxy across RO and reanalysis, leveraging RO's sensitivity to moisture.

Where P_d (hPa) is the dry atmospheric pressure , e (hPa) is the water vapour pressure, and T (K) is the absolute temperature. The first term of is the dry term (Ndry) of the radio refractivity, and the second and third terms of this Equation are the wet terms(Nwet). Since dry and wet terms contribute to air refractivity, water vapour pressure (temperature) profiles require distinct temperature (water vapour pressure) information. The data is obtained directly as one of the datasets from the "wetPrf" profiles of the RO data. The variations in mean refractivity obtained from 2011 to 2021 are presented in the result section. Also, N was estimated from the temperature and relative humidity at 850 hPa using from two reanalyses sources: the NCEP and EAR5 temperature and relative humidity data .

2.3 Calculation of gravity wave potential energy

2.4 The GW potential energy

The atmospheric temperature profile (T) from RO is a function of height (h), which consists of the background temperature profile $\overline{T}(z)$ and the fluctuating component $T'(z)$. The E_p has been used as a proxy for studying GW activities, as presented by ? and ?, and is given byTo quantify GW activity in the stratosphere, we calculate the potential energy (Ep) per unit mass from RO temperature profiles. This approach follows established methodologies (**???**) and provides a robust measure of GW activity. The potential energy is calculated as:

$$E_p\mathrm{Ep} = \frac{1}{2}\left(\frac{g}{N}\right)^{22}\left(\frac{T'}{\overline{T}}\frac{T'}{\overline{T}}\right)^{2,2} \tag{2}$$

Where where g is the acceleration due to gravity ($9.8\,\mathrm{m\,s^{-2}}$), N is the Brunt-Väisälä frequency, and $\bar{T}$, and T' are the local background temperature profiles and the temperature fluctuation profiles caused by GW activities, respectively. The E_p calculation is based on the accurate extraction of T', which Brunt-Väisälä frequency, T' is the temperature perturbation associated with GW, and $\overline{T}$ is the background temperature profile. The temperature perturbation is calculated by subtracting the background temperature from the observed temperature:

$$T' = T - \overline{T} \tag{3}$$

The Brunt-Väisälä frequency, which characterizes the stability of the atmosphere, is given by:

$$T'N^2 = T-,\frac{g}{\overline{T}}\left(\frac{\partial\overline{T}}{\partial z} + \frac{g}{C_p}\right) \tag{4}$$

And N is given as follows:

$$N^2 = \frac{g}{\overline{T}}\left[\frac{\partial\overline{T}}{\partial h} + \frac{g}{C_p}\right],$$

C_p is the where z is the altitude and C_p is the specific heat capacity of the dry air at constant pressure , and h is the altitude. The GW E_p is calculated using . The E_p depends only on the raw temperature profile, which can be separated into ($1004\,\mathrm{J\,kg^{-1}\,K^{-1}}$).

A critical challenge in calculating Ep is the accurate separation of GW-induced temperature perturbations (T') from the background temperature ($\overline{T}$)and the temperature fluctuation (T') . In calculating E_p, the T' is the main issue that requires careful attention (**?**). The raw temperature profile obtained from RO is first interpolated at 100 m intervals along the altitudes. Each temperature profile is divided into cell sizes of $20° \times 10°$ of longitude and latitudebetween 10 and 50 km of altitudefield ($\overline{T}$). Traditional methods such as polynomial fitting, running means, or simple band-pass filtering have significant limitations: they can introduce artificial perturbations at the edges of filtering windows, fail to adapt to varying atmospheric conditions, and may not effectively distinguish GWs from other types of wave (**?**).

To address these limitations, we implement a more sophisticated approach using the continuous wavelet transform (CWT) (**??**). Our procedure consists of the following steps: we first interpolate the raw temperature profiles from RO measurements into a regular vertical grid with 100-m intervals from 10 to 50 km altitude. The profiles are grouped into spatial cells of $20° \times 10°$ (longitude × latitude), and the mean temperature of each grid is calculated . The profile is calculated for each cell. This spatial averaging helps reduce noise and provides more robust estimates of the background state. We apply a CWT with a Morlet wavelet to each mean temperature profileis decomposed using a continuous wavelet transform (CWT) (**??**) to obtain the . The CWT decomposes the temperature profile into components on a spectrum of vertical scales. The background temperature ($\overline{T}$) . The $\overline{T}$ is $\overline{T}$) is reconstructed by including only components with vertical wavelengths longer than 10 km, effectively separating the large-scale background structure from smaller-scale wave perturbations. This background temperature is then interpolated back to the positions of the original temperature profiles and subtracted from the raw temperature profile using to obtain T'. The variations of the mean E_p obtained from 2011 to 2021 are presented in Equation 3 to obtain the temperature perturbations (T'). Finally, Ep is calculated using Equation 2 at various altitudes, with our analysis focusing mainly on 20 km altitude, where the quality of RO data is high and the influence of tropospheric water vapour is negligible.

2.4 Method of identifying ITCZ and maximum Ep

The water vapour contributes to greater atmospheric refractivity (N)than the atmospheric temperature in the upper troposphere region approximately 8-12 km. Nonetheless, A significant methodological consideration is the RO satellite's refractivity data is precise from the surface to 40 km. It also contains temperature and water vapour data (**??**). **?** and **?** used RO refractivity to locate the ITCZ. It is worth noting that changes in the lower troposphere can considerably impact refractivity. In contrast, temperature regulates refractivity in the higher troposphere due to less water vapour input. As a result, it is feasible to detect the ITCZ from the surface to the high troposphere using refractivity, a unique metric available only directly from RO satellites.potential contamination of GW signals by other wave types, particularly equatorial Kelvin waves, which can have vertical wavelengths that overlap with the GW spectrum (typically 2-10 km for GW versus 5-15 km for Kelvin waves) (**??**). To minimize this contamination, we implement an additional filtering step that targets the characteristic properties of Kelvin waves: eastward propagation, zonal wavenumbers 1-3, and periods of 4-23 days (**?**). This approach makes it possible to isolate GW disturbances

from other types of waves, although a certain amount of residual contamination near the equator cannot be entirely ruled out by analyzing the 1D profile alone..

~~In this study, we employed a similar procedure used by ? to locate the ITCZ position concerning the~~ Our CWT-based method offers several advantages over simpler filtering techniques. First, it adapts to varying atmospheric conditions rather than applying fixed cut-offs. Second, it minimizes edge effects that can introduce artificial perturbations. Third, it provides better separation of wave types based on their scale characteristics. These advantages are particularly important when analyzing GW activity across different seasons and geographical regions, where background conditions and wave properties can vary significantly. The resulting Ep values represent the energy density associated with GWs and serve as our primary metric for GW activity in the stratosphere. This approach can resolve GWs with vertical wavelengths greater than approximately 2 km (twice the vertical resolution of the ~~satellite data by fitting Gaussian functions in our methodology. We also used it to determine the position of the maximum GW Ep. This approach determines the meridional distribution of refractivity and~~ interpolated profiles) and less than 10 km (the cutoff used to separate background and perturbation components). This range captures most stratospheric GWs while minimizing contamination from larger-scale waves and smaller-scale noise. The results are shown primarily for 20 km altitude. Using temperature profiles for Ep ~~. The peak position, location, and width (full-width half maximum) of the Gaussian are computed using the refractivity from RO , NCEP, and ERA5 data~~ calculation is standard practice for stratospheric GW analysis of RO (e.g., **??**).

2.4 Method for Identifying ITCZ and Maximum Ep Locations

To objectively determine the latitudinal positions of the ITCZ and stratospheric GW potential energy maxima, we implemented a Gaussian fitting approach similar to that employed by **?**. This method identifies the peak positions in the meridional distributions of refractivity for ITCZ and Ep ~~data grids for each longitude.~~

~~The data series includes global refractivity and Ep observations with~~ for GW activity. We first gridded the RO and reanalysis data in a global $2^\circ \times 2^\circ$ ~~longitude and latitude grid resolution. We eliminate the irregular border layersby calculating the mean of the refractive index~~ longitude-latitude resolution. To minimize the effects of orography and irregular boundary layers, we calculated mean values for both refractivity and Ep at each 10° ~~latitude along the longitudes to reduce the effects of orography. This approach~~ longitude band across all latitudes. This preprocessing was applied to ~~the~~ monthly averages of ~~the refractive index~~ refractivity at 850 hPa (serving as our ITCZ proxy) and Ep at ~~a pressure level of 850 hPa. The parameters of the refractive index distribution are determined by fitting a Gaussian function at each longitude, provided as~~20 km altitude (representing stratospheric GW activity).

For each longitude λ and month t, we fit a Gaussian function to the latitudinal distribution of refractivity or Ep between 30° S and 30°N. The fitting function takes the form:

$$Qf(\phi,\lambda,t) = Q_{\max} e^{-\frac{(\phi-\phi_{\max})^2}{2\sigma_Q^2}} A(\lambda,t) \exp\left(-\frac{(\phi-\phi_{\max}(\lambda,t))^2}{2\sigma(\lambda,t)^2}\right) + B(\lambda,t) \tag{5}$$

where $Q(\phi)$ represents the meridional refractive index at each longitude; $\phi_{\max}$, represents the meridional where ϕ is latitude, $\phi_{\max}(\lambda,t)$ represents the latitudinal position of the particular refractive index at a given longitude; $Q_{\max}$ represents the highest value of refractive index, and σ_Q^2 represents the meridional variance of refractive indexpeak ITCZ or Ep maximum, $A(\lambda,t)$ is the amplitude indicating the strength of the feature, $\sigma(\lambda,t)$ is the width parameter representing the meridional extent, and $B(\lambda,t)$ is the background value.

To perform the Gaussian fitting using a non-linear least-squares method with several constraints to ensure physically meaningful results, the following steps were taken. First, the fit was restricted to the tropical latitude band (30°S to 30°N) to focus on the primary ITCZ and GW activity regions. Second, a minimum coefficient of determination (R^2) value of 0.7 was required for a valid fit, ensuring that the Gaussian model adequately represented the data, and the standard deviation of the Gaussian (σ) was restricted to be between 5° and 15° to exclude unrealistically narrow or wide distributions.

2.5 Trend analysis method

The linear trend of The method is particularly effective for identifying the ITCZ in regions where it forms a well-defined band, such as over the open oceans. However, it may be less reliable in regions with complex convective patterns, such as over the Maritime Continent, or in areas with double ITCZ structures. In such cases, the fit identifies the dominant peak, which typically corresponds to the stronger convective zone. By applying this consistent methodology to the refractivity and Ep distributions, we can directly compare the latitudinal positions and characteristics of ITCZ and stratospheric GW activity, allowing analysis of their spatial relationships and temporal covariability.

To illustrate this approach, Figure 2 shows the application of our method for a specific longitude (76° W) in 2016, showing the latitudinal distributions of refractivity and Ep during December-January-February (DJF) and June-July-August (JJA), together with their respective Gaussian fits.

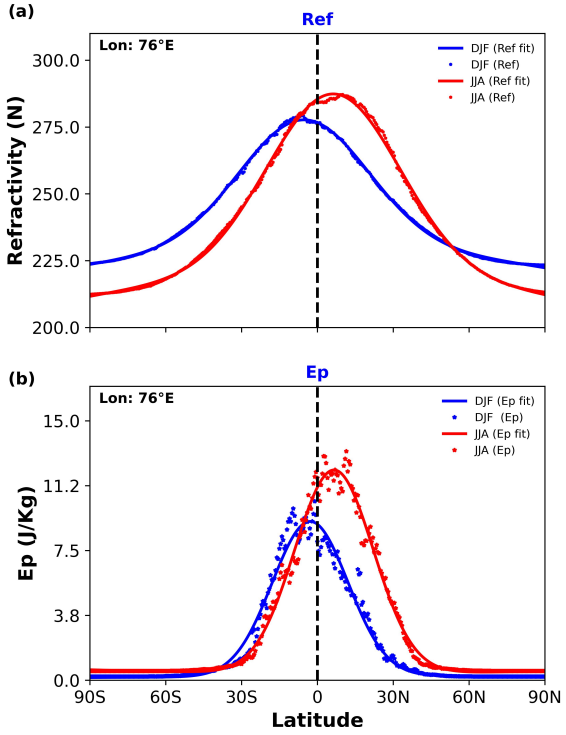

Figure 2. Latitudinal distribution of **(a)** refractivity (N-units) and **(b)** gravity wave potential energy (Ep, J/kg) at 76°W during December-January-February (DJF, blue) and June-July-August (JJA, red) in 2016. Thick lines show the Gaussian fits used to determine the latitudinal positions of the ITCZ and Ep maxima.

Both refractivity and ~~refractivity zonal mean time series and the responses to ENSO, MJO, and QBO wind are calculated for each longitude using the~~ Ep show similar latitudinal distributions, with peaks near the equator during DJF and a northward shift to approximately 15°N during JJA. This seasonal migration is consistent with the expected movement of the ITCZ following the region of maximum solar heating. The close correspondence between refractivity and Ep distributions suggests that ITCZ and stratospheric GW activity are closely linked, with GWs likely generated by deep convection within the ITCZ.

2.5 Trend Analysis Method

To investigate the modulation by climate variability modes, we use the following standard indices: The Multivariate ENSO Index Version 2 (MEI.v2) shown in Figure 3a, obtained from the NOAA Physical Sciences Laboratory (https://psl.noaa.gov/enso/mei/). We use monthly values derived from the bimonthly index (**?**). Positive values indicate El Niño conditions, while negative values indicate La Niña conditions. The Real-time Multivariate MJO (RMM) index is shown in Figure 3b (**?**). We used the monthly amplitude, calculated as $\sqrt{RMM1^2 + RMM2^2}$, obtained from the Australian Bureau of Meteorology (http://www.bom.gov.au/climate/mjo/graphics/rmm.74toRealtime.txt). Higher amplitude indicates stronger MJO activity. For the

Quasi-Biennial Oscillation (QBO), we used the monthly mean zonal winds at 30 hPa (~24 km) and 50 hPa (~21 km) from radiosonde observations over Singapore, as illustrated in Figure 3c. These data were obtained from the Karlsruhe Institute of Technology's Atmosphere and Climate Data Hub (https://www.atmohub.kit.edu/english/807.php). To remove regression uncertainty, the QBO zonal wind data at 30 mb and 50 mb were normalized. These modes of climate variability are presented in Figure 3, which shows the reference time series used in the regression analyses.

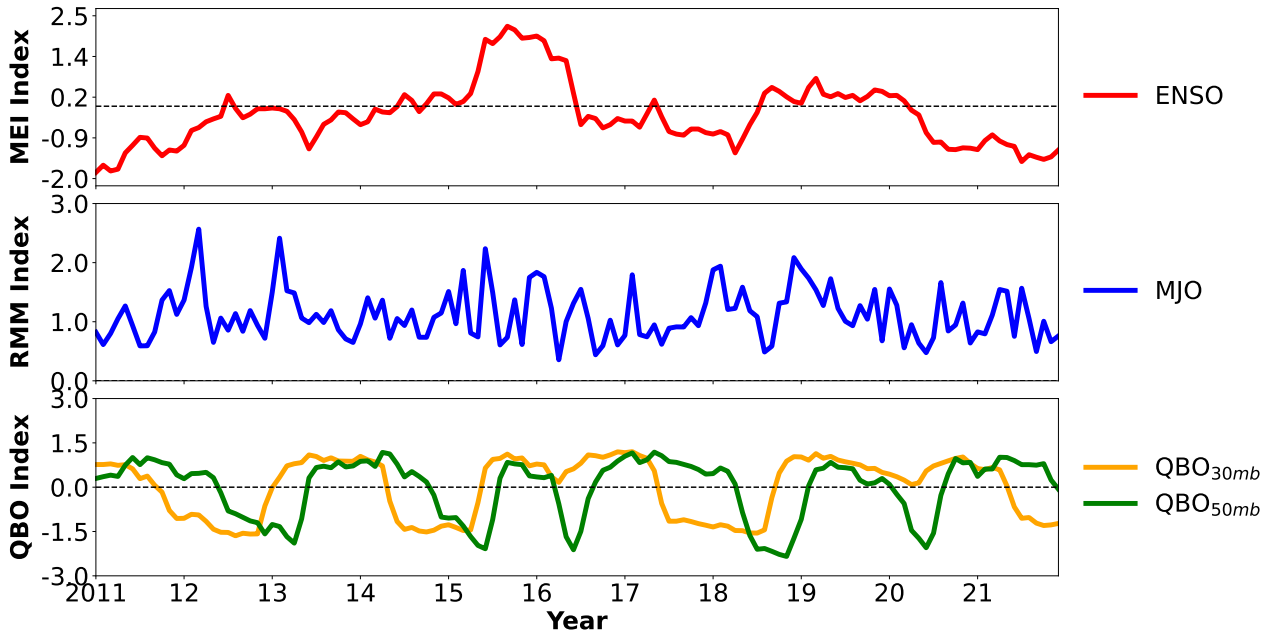

Figure 3. Reference time series from 2011 to 2021 used for the regression analyses. **(a)** Multivariate ENSO Index (MEI) characterizing the ENSO signal (red), **(b)** Amplitude of Real-time Multivariate MJO indices (RMM) 1 and 2 characterizing the MJO signal (blue), and **(c)** Normalized zonal winds at 30 hPa (24 km, orange) and 50 hPa (21 km, green) over the equator characterizing the QBO.

To analyze trends in ITCZ position and GW activity and their relationships with climate variability modes, we employed a multivariate linear regression (MLR) approach ~~(**???**). The MLR can determine the link between one~~ (**???**). This method allows us to determine the relationship between a dependent variable (e.g., ITCZ position or Ep) and ~~two or more~~ multiple independent variables (e.g., time, ENSO, MJO, and QBO ~~wind~~indices). The MLR ~~method's equation is~~ equation is formulated as follows:

$$\Psi(t_{i,j}) = \mu + \alpha_0 t_{i,j} + \alpha_1 \cdot QBO_{30hPa}(t_{i,j}) + \alpha_2 \cdot QBO_{50hPa}(t_{i,j}) + \alpha_3 \cdot MJO(t_{i,j}) + \alpha_4 \cdot ENSO(t_{i,j}) + \text{Residual}, \quad (6)$$

With $i = 2011, 2012, \ldots, 2021$; and, $j = 1, 2, \ldots, 12$

~~The~~ where Ψ represents the monthly zonal mean value of the parameter of interest (ITCZ position, Ep ~~or refractivity is represented as Ψ, the monthly values denoted as $(t_{i,j})$ (where (i)~~ maxima position, refractivity value, or Ep value); $t_{i,j}$

denotes the time in months (where i is the year and ~~(j)~~ j is the month)~~, and the quantity~~ ; μ represents a constant ~~Ep value. The parameter α_0, which depicts the change in GW parameters over time, represents the monthly zonal Ep or refractivity linear trend from 2011 to 2021. The parameters α_1~~term; α_0 represents the linear trend over time; and α_1 through α_4 represent the regression coefficients for the normalized QBO at 30 hPa, normalized QBO at 50 hPa, ~~α_2, α_3, and α_4 show the relationship between the timeseries of the Ep or the refractivity parameters and the time series of the four indices, depicting the monthly GW parameter's zonal response to QBO at 30 hPa and 50 hPa,~~ MJO, and ENSO indices, respectively. The residual ~~of the regression model can be utilized to estimate each coefficient's~~ term represents the unexplained variance in the regression model. The standard deviation and p-value ~~. This estimation can be achieved~~ for each coefficient were estimated using the variance-covariance matrix and the Student's t-test (**??**). ~~presents the reference time series of ENSO, MJO, and QBO from 2011 to 2021. The bi-monthly Multivariate ENSO Index (MEI) values in a show the temporal variations of the ENSO phases (?). The monthly Real-time Multivariate MJO Index (RMM) values in b show the temporal variations of the RMM phases. The RMM is calculated by projecting 20-96 day filtered OLR, which includes all eastward and westward wave numbers, onto daily spatial EOF patterns of 30-96 day eastward filtered OLR (?). In c, the reference time series for 30 hPa and 50 hPa are the temporal fluctuation of QBO zonal-mean zonal wind across the equator (?). The QBO data are from radiosondes (obtained from the Meteorological Service Singapore Upper Air Observatory (1.34°N, 103.89°E) , NASA (National Aeronautics and Space Administration)/GMAO (Global Modeling and Assimilation Office)assimilated data, and NASA satellites through the NASA earth-data site.~~ A p-value threshold of 0.05 was used to determine statistical significance.

~~Reference time series from year 2011 to 2021 used for the regression analyses. **(a)** Multivariate ENSO Index (MEI) to characterize the ENSO signal (red), **(b)** The amplitude of Real-time Multivariate MJO indices (RMM) 1 and 2 to characterize the MJO signal (blue), and **(c)** 30 hPa (24 km, orange) and 50 hPa (21 km, green) zonal winds over the equator to characterize the QBO.~~

3 Results

~~The~~

3.1 Climatology and Seasonal Variability of ITCZ and GW Ep

First, we examine the mean spatial distribution and seasonal variation of the ITCZ proxy (refractivity at 850 hPa) and stratospheric GW activity (Ep at 20 km). Figure 4 shows the global distribution of refractivity values at 850 hPa from RO, ERA5 ~~, and NCEP at 850 hPa~~and NCEP data for 2021, integrated over a $2° \times 2°$ latitude-longitude grid~~for the year 2021, is shown in . In the paper, we divided the seasons into December–January–February (DJF), March-April-May (MAM), June–July–August (JJA), and September-October-November (SON). The analysis is presented for boreal winter (DJF) and summer (JJA). We observed that refractivity (N) varied between 260 and 290 N units (a). In contrast, refractivity from ERA5 and NCEP ranged from 240 to 310 N units (a and b, respectively), capturing the Intertropical Convergence Zone (ITCZ) around the equatorial region. At the 850 hPa pressure level, cloud-top heights are inferred from N profiles. Convective regions are prominent across~~

~~the Indian Ocean, the western Pacific, Africa, and South America during DJF. The higher refractivity values shift to the~~ . All three datasets effectively capture the ITCZ as a band of enhanced refractivity near the equator, which shifts seasonally between hemispheres. Consistent with known climatology, the ITCZ is located predominantly in the Southern Hemisphere (SH) ~~in DJF (a) and to~~ during DJF (Figure 4a, c, e) and shifts significantly into the Northern Hemisphere (NH) ~~in JJA (b). Key regions with relatively high refractivity (highlighted with red circles) include South Americaand Africaduring DJF, as well as Mexico, the southern United States, and the Asian monsoon region during JJA. The refractivity values from RO,~~ during JJA (Figure 4b, d, f). Maximum refractivity values are typically found over tropical landmasses (South America, Africa, and the Maritime Continent) and warm ocean pools (West Pacific).

Although the overall patterns are similar, RO-derived refractivity (Figure 4a, b) generally shows slightly lower peak values (range $\sim$ 260-290 N units) compared to ERA5 ~~, and NCEP exhibit similarities, although ERA5 and NCEP tend to show slightly higher values, indicating an overestimation of refractivity by approximately two tens of N units compared to RO~~and NCEP (range $\sim$ 240-310 N units), particularly noticeable in the reanalysis maxima (circled regions). These differences likely result from variations in spatial resolution, observational coverage, and data assimilation techniques between satellite-based RO measurements and model-based reanalysis products. The RO data show finer-scale structures and stronger gradients compared to the reanalyses, particularly in regions with complex topography or limited conventional observations.

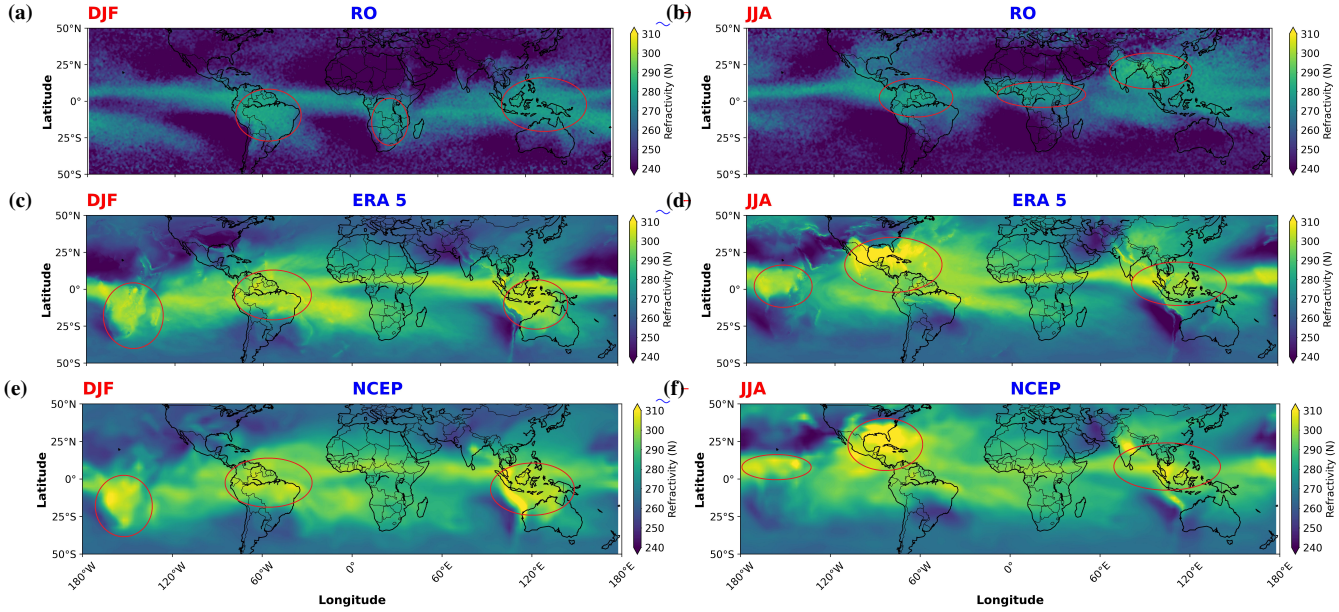

Figure 4. ~~The~~ Global distribution of refractivity ~~in 2021~~ (N-units) at 850 hPa during December-January-February (DJF; left column: **a, c, e**) ~~**(a, c, e)**~~ and June-July-August (JJA; right column: **b, d, f**) ~~**(b, d, f)**~~ ~~at 850 hPa. The circled regions~~ in 2021. Data are ~~the regions of high concentrations of refractivity. (**a** and **b) The refractivity was obtained~~ derived from RO ~~for DJF and JJA. (**c** and **d**~~**a, b**)~~The refractivity is estimated from~~ , ERA5 ~~for DJF and JJA. (**e** **c, d**)~~, and ~~f~~NCEP (**e, f**)~~The~~ . Circled regions highlight areas of high refractivity ~~estimated from NCEP for DJF~~ concentration associated with the ITCZ and ~~JJA~~monsoon systems. Note the seasonal shift of the high-refractivity band between hemispheres.

~~The~~ Figure 5 presents the global distribution of the GW potential energy (Ep~~values measured at 20 km in~~) at 20 km altitude for DJF and JJA in 2021~~(a year with the highest number of profiles) is given in . The Ep contour intervals are 0 - 15 Jkg^{-1} at 20 km. Higher values of ~15 Jkg^{-1} at 20 km for both seasons are seen towards the equator and decrease towards the polar regions~~ , derived from RO temperature profiles. ~~The high~~ Elevated Ep values ~~in the equatorial region ()are attributable to the significant quantity of deep convective activity caused by high temperatures and humidity in that region. In ,~~(~5-15 Jkg^{-1}) are concentrated in the tropics and subtropics, broadly overlapping with the regions of high convective activity suggested by the refractivity maps. The Ep field shows distinct seasonal patterns with several key features: First, an equatorial band of enhanced Ep that shifts seasonally between hemispheres, broadly following the ITCZ. During DJF (Figure 5a), high Ep values ~~at tropical and subtropical latitudesare substantial in all the months presented. This might be related to more convection than predicted and partially due to equatorial waves. The GW~~ are observed in equatorial South America, Africa and the western Pacific. During JJA (Figure 5b), the enhanced regions Ep ~~is considerably high in JJA~~ shift northward, with pronounced features over Central America, the Sahel region, and South Asia. Second, the strong Ep values in the winter hemisphere mid to high latitudes, particularly in the Northern Hemisphere during DJF. This feature is associated with the polar

night jet, which allows more efficient vertical propagation of GWs generated by various sources, including orography and jet streams. Third, localized Ep enhancements on major mountain ranges, such as the Andes, Rockies, and Himalayas, which are persistent sources of orographic GWs. A distinct feature of JJA are the high Ep values over the southern Andes (30°S-50°S)~~and diminishes eastwardin JJA b. This occurrence might be owing to the eastward spread of~~ , which diminish eastward, likely associated with orographic mountain waves ~~created by the Andes'~~ generated by the north-south ~~distribution, primarily due to low-level westerlies and the persistent jet (?). We found a similarity between the Asian monsoon and the eastern Pacific Ocean in the refractivity in and the high values of the GW Ep in . The equatorial stratospheric GW activity is centred towards the equator over Southern America and Africa (), compared to the result in . Moderate values of Ep (~ 6-7 J kg^{-1}) showing equatorial~~ orientation of the Andes and the strong westerly jet in this region (?). Lastly, a notable equatorial maximum over the western Pacific was observed during both seasons, which is likely associated with persistent deep convection in this region.

The spatial patterns in Figure 5 are broadly consistent with previous global GW climatologies derived from RO (e.g., ???). The spatial correlation between tropical Ep maxima and the high-refractivity regions associated with ITCZ (Figure 4) suggests a direct link between tropospheric convection and stratospheric GW activity~~are seen over Mexico and the USA with high refractivity values in JJA~~. However, the Ep distribution also shows features that are not directly related to the ITCZ, indicating the importance of other GW sources and propagation conditions.

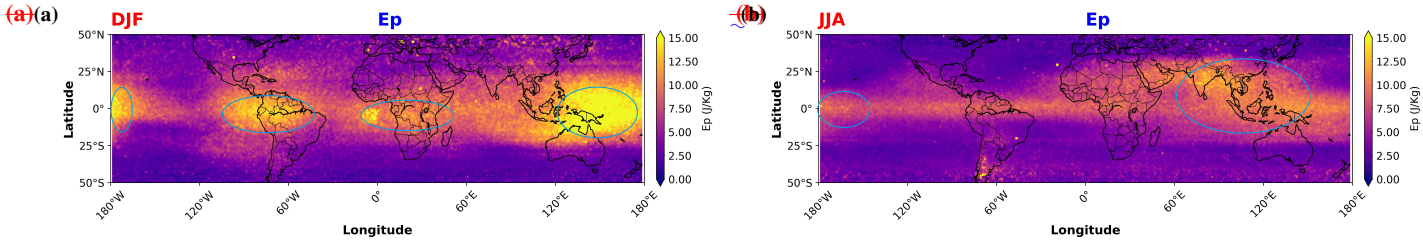

Figure 5. ~~The~~ Global distribution of gravity wave potential energy (Ep~~variations in 2021~~ , J kg^{-1}) at 20 km altitude during **(a)** December-January-February (DJF) ~~**(a)**~~ and **(b)** June-July-August (JJA) ~~**(b)** at 20 km~~in 2021, derived from RO temperature profiles. ~~The circled~~ Circled regions ~~are the regions~~ highlight areas of high ~~concentrations of~~ Ep concentration, often associated with deep convection or orography (e.g., Andes in JJA).

3.2 ~~The ITCZ and Ep maxima~~

~~Based on the approach used by ?? to identifying ITCZ and maximum Ep, we report the morphology, inter-annual variability, and possible trends of the refractivity-derived ITCZ and the local maxima of the equatorial stratospheric GW Ep distribution. The emphasis is on DJF and JJA. For example, the technique based on monthly mean Ep and refractivity at 850 hPa is validated over DJF and JJA. The weighted zonal distribution of Ep and refractivity at 76°W in 2016 (location and years were chosen at random) and the resulting Gaussian fit~~ To quantitatively analyze the relationship between the ITCZ and stratospheric GW activity, we applied the Gaussian fitting method described in Section 2.4 to identify the latitudinal positions of the ITCZ

(using refractivity) and the maximum GW potential energy. Figure 6 shows the longitudinal variation of these peak locations averaged over the 11-year period (2011-2021) for DJF and JJA~~are shown in . The distribution of Ep and refractivity is similar, with the highest near the equator during JJA and amovement towards the north (~15°N for both Ep and refractivity) in JJA~~ . ~~Nonetheless, there is a slight variation in the northern latitudes in JJA. The mean maximum location was determined by refractivity in 2016 throughout the DJF and JJA seasons, as shown in . During DJF, the maximum location changes to the SH to about 7°S for both Ep and the refractivity in 2016 at 76°W.~~

~~Latitudinal distribution of **(a)** refractivity and **(b)** Ep observed during December- January-February (DJF) and June-July-August (JJA) at 76°W in 2016 at 800hPa. Thick lines show the Gaussian fit.~~

~~The ITCZ's mean shape and inter-annual seasonal variations, as determined by refractivity data and the seasonal maximum Ep, are presented in . The inter-annual variability of ITCZ using RO~~ The mean position of ITCZ (Figure 6a) clearly shows the seasonal shift: located around 5°S-10°S during DJF (green lines) and shifting to 5°N-15°N during JJA (red lines). The magnitude of the shift varies with longitude, being largest over Africa and the Indian Ocean. RO (solid lines), ERA5 (dashed), and NCEP ~~data was computed across DJF and JJA months from 2011 to 2021 (11 years of observation) . Inter-annual variability has shifted by nearly ~5° - 15° north and south. Throughout the 11 years of data, the ITCZpositions are practically similar. There is a slight difference in the ITCZs obtained from RO, ERA5, and NCEP. From 2011 to 2021, b depicts the mean positions of maximum refractivity and Ep for DJF and JJA. Throughout DJF and JJA in both NH and SH, the mean distribution of ITCZ exhibits a slightly noticeable movement. The ITCZ is positioned about 5°S in DJF and approximately 7°N in JJA. The ITCZ position moves by 10° between DJF and JJA throughout the global oceanic areas. The SON and MAM are the transition seasons between DJF and JJA, so their results are expected to be similar. Apart from seasonal oscillations, the ITCZ has inter-annual shifts in location and intensity.~~ (dotted lines) generally show good agreement in the mean position of the ITCZ, although there are some regional differences, particularly the somewhat smoother structure of the NCEP, due to its coarser resolution.

~~**(a)(b)**ITCZ and Ep maxima are located from 11 years of refractivity data and Ep maxima of the equatorial stratospheric GW at 20 km. **(a)** The global inter-annual variability of ITCZ lines during JJA and DJF of the refractivity and Ep maxima. **(b)** The estimated mean of the ITCZ and Ep maxima lines during JJA and DJF.~~

~~The global equatorial stratospheric GW Ep maxima also showed the same seasonal differences as the ITCZ .~~ The ~~global equatorial stratospheric GW~~ mean location of the stratospheric Ep ~~maxima (b) showed more consistency in the NH and SH with much closer spacing than the ITCZ. We find two essential features that distinguish the~~ maximum (Figure 6b) also shows a clear seasonal migration, generally following the ITCZ shift but with some notable differences. The peak Ep ~~morphology from the ITCZ. The first one is related to the shift of Ep position by 5° between DJF and JJA. The distance between the Ep maxima is consistent, with JJA moving northward and DJF southward. Secondly, the Ep maxima in DJF and JJA showed two points of convergence over the South American Amazon and the equatorial Pacific. These convergences do not exist in MAM or SON. The South American Amazon and Central American climate are the broadest deep convective zones around the globe (**???**), and these could be the reason for the convergence of Ep maxima. It is also noted that the convergence over the Pacific Ocean could result from the double ITCZ prevailing in this region (**???**). This feature is also seen in over the Pacific Ocean. The most significant gap in seasonal localization between the ITCZ in~~ (solid green/red lines) tends to stay closer to the

equator compared to the ITCZ proxy, especially during JJA over the Atlantic and Africa. The latitudinal separation between the DJF and JJA ~~is seen over Africa and the Indian Ocean to the east, also observed in~~ Ep ~~maxima. This result could be due to the Sun being directly overhead at the Tropic of Capricorn during DJF in the Southern Hemisphere (SH) , leading to a shift of the Intertropical Convergence Zone (ITCZ) and the convergence of trade winds further into the SH. This results in the formation of deep convective cloud systems. During this period, a low-pressure area develops south of the equator, while a high-pressure area forms north of the equator, driving the ITCZ southward due to clear-sky forcing. Conversely, when the Sun is directly overhead at the Tropic of Cancer during JJA, the ITCZ shifts northward, concentrating trade winds in the Northern Hemisphere (NH) , which could also influence the generation of equatorial stratospheric GWs~~peaks is typically smaller (~5° -10°) than the ITCZ shift (~10°-20°). This suggests that while convection associated with the ITCZ is a primary source, the observed stratospheric GW maximum is also influenced by propagation effects (including horizontal propagation) and potentially filtering by stratospheric winds, leading to a peak location that does not perfectly mirror the tropospheric source region (**?**).

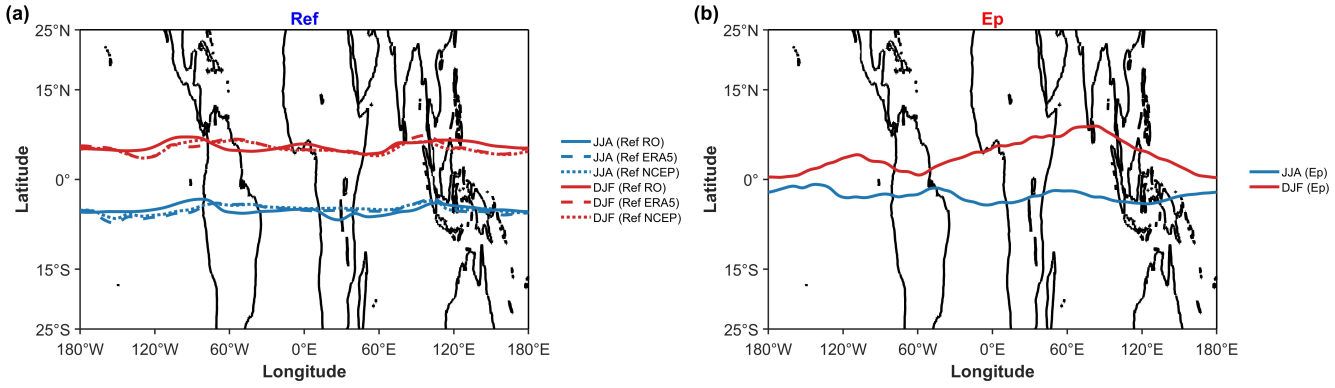

Figure 6. Longitudinal variation of the 11-year (2011-2021) mean latitudinal location (ϕ_{max}) of maxima derived from Gaussian fits. **(a)** Mean ITCZ location derived from refractivity at 850 hPa for DJF (green lines) and JJA (red lines). Solid lines are from RO, dashed from ERA5, dotted from NCEP. **(b)** Mean GW Ep maximum location derived from RO temperature at 20 km for DJF (green solid line) and JJA (red solid line). Note the consistent seasonal migration in both ITCZ and Ep maxima.

3.2 ~~Equatorial stratospheric GWs, ITCZ and other related parameters~~

~~In this section, we compare the two main parameters (i.e., specific humidity and vertical wind) in different seasons, which should show whether the locations of the derived~~ To further explore the relationship between ITCZ, Ep, and other meteorological fields often associated with convection, Figure 7 compares the mean ITCZ and Ep maxima ~~match. The first parameter is the mean~~ locations with specific humidity, ~~overlaid in a and b with the ITCZ, Ep maxima, and OLRat 200 - 250 W m^2.~~

The specific humidity, the vertical wind velocity, and the OLR are taken at 800 hPa. In the lower troposphere, atmospheric humidity is an important parameter. The amount of water vapour per air volume determines the humidity, which is determined by evaporation, advection, and precipitation. Our results show perfect agreement between OLR and vertical velocity, and OLR. The high specific humidity (Figure 7a, b) aligns well with the ITCZ location derived from refractivity (cyan line), confirming the moisture-based proxy. The ITCZ position generally aligns well with regions of maximum specific humidity, especially in DJF. There are exceptions in JJA, particularly over the southern United States of America (USA), where specific humidity is high outside the OLR, despite the region experiencing opposite seasons. The OLR shows that the ITCZis a wandering, thin band of clouds around the equator.

As previously reported, **?** used specific humidity to determine the position of the global ITCZ, which was later confirmed by **?**. For example, **?** showed a positive relationship between lower tropospheric humidity and tropical deep convection, the latter associated with radiative heating (cooling)at the surface (top). **?** consistently found extensive evaporation on both sides of the ITCZ that carries water vapour into the ITCZ, a first indication of the link between tropical deep convectionin the ITCZ and moisture in the lower troposphere. We also observed divergence of the ITCZfrom the peak specific humidity values over the African landscape and the Indian Ocean. This phenomenon will be discussed in the discussion section. The closest match between the ITCZ and oceans, consistent with the ITCZ's characteristic as a zone of convergence. Regions of strong upward motion (negative vertical velocity, Figure 7c, d) and low OLR (contours in Figure 7a, b, e, f), both indicative of deep convection, also generally coincide with ITCZ.

The mean Ep maxima was observed over the Asian monsoon.

Another approach to identifying the ITCZ is wind convergence, later associated with the vertical wind by **?**. The vertical wind indicates the ITCZ position, which is identical to the OLR position. c and d shows the 2D variation of the vertical wind superimposed on the ITCZ and maximum location (magenta line) is often located equatorward or slightly poleward of the peak convective indicators, again highlighting the role of propagation and potentially wave filtering. For example, in South America in JJA (Figure 7d, f), the Ep maxima in all seasons. The black contour lines show the vertical velocity at 0 $\mathrm{m\,s^{-1}}$, which can also be used as a proxy for the ITCZ (**?**). The zero vertical wind can be considered the convergence of the wind. In all seasons, the ITCZis mainly within the wind convergence. As mentioned earlier, there is a slight variation between the ITCZ and the wind convergence over Africa and the Indian Ocean. maximum appears somewhat south of the main ITCZ/convection band. Interestingly, the Ep maximum fits perfectly within maxima position shows an even closer alignment with the zero vertical wind. During the JJA, velocity contour, particularly over the Pacific and Atlantic Oceans. This suggests that GW activity may be enhanced not only by deep convection but also by the vertical wind shear associated with the boundaries of convective regions.

The Ep maxima line shifts southward over South America, further from the ITCZ and wind convergence. This phenomenon could be a consequence of ENSO or other tropical dynamics.

The mean global specific humidity (in $\mathrm{g\,kg^{-1}}$), vertical wind velocity (in $\mathrm{Pa\,s^{-1}}$), and Ep (in $\mathrm{J\,kg^{-1}}$) from 2011 to 2021 in December-January-February (DJF) and June-July-August (JJA). (**a** and **b**), The mean global specific humidity was overlaid with the Ep maxima (red solid line) and ITCZ (purple solid line) during DJF and JJA, respectively. The black contour lines are

the OLR at 200 - 250 $\mathrm{W\,m^{-2}}$. (**c** and **d**), The mean global vertical velocity was overlaid with the Ep maxima (red solid line) and ITCZ (purple solid line) (top row) during DJF and JJA, respectively. The black contour lines are the vertical velocity at 0 $\mathrm{m\,s^{-1}}$ (middle row). (**e** and **f**), The mean global Ep was Ep overlaid with the ITCZ (purple solid line) during DJF and JJA, respectively. The black contour lines are the OLR at 200 - 250 $\mathrm{W\,m^{-2}}$. The specific humidity, the vertical wind velocity, and the OLR are taken at 800 hPa.

To verify that the location of the ITCZ derived from the refractivity field and OLR was consistent, we plotted the refractivity field and Ep maxima on the mean Ep distribution shown in e and f. Our result showed that the ITCZ derived from the refractivity field coincides with the equatorial OLR at 200 - 250 $\mathrm{W\,m^{-2}}$. It should be noted that OLR is electromagnetic radiation with wavelengths in the range of 3 - 100 µm radiated from the Earth and its atmosphere into space as thermal radiation. The OLR represents the atmosphere's total radiation, making it vital to Earth's energy budget (**?**). The equatorial OLR is a proxy for estimating the global deep convective zones, sometimes called the ITCZ (**??**). The mean Ep fluctuation has the same features described in above. In eand f, the equatorial stratospheric GW Ep in DJF is mainly distribution (Figure 7e, f) exhibits clear seasonal patterns, with high values concentrated in four regions globally. Ep values are high regardless of land and sea proximity to deep convection areas. Deep convection can be detected in Africa, main regions during DJF: equatorial South America, Asia, and the Indian and Pacific Oceans. Our results show a one-to-one correlation between equatorial stratospheric GW activity and deep convection in the band of latitudes where deep convection is detected. This result agrees with Africa, the results of **??**.

In JJA (e and f), equatorial stratospheric GW is mainly concentrated in the Maritime continent and the western Pacific. During JJA, the regions of enhanced Ep shift northward, with notable concentrations over the eastern part of Africa, Asiathe Asian monsoon region, and the Indian and Pacific Oceans. equatorial stratospheric GW activity has shifted toward the NH, concentrating mainly on India and Southeast Asia, then dropping toward the Pacific. This phenomenon is seen as a result of the ITCZand trade winds in this region, as reported earlier. The equatorial stratospheric GW decreased mainly over western and equatorial South America and did not precisely follow the ITCZ path as observed in DJF. This result could result from ENSO producing more dryness over tropical South America in JJA (**?**). This phenomenon produces a narrower band of equatorial stratospheric GW activity concentrated along a line in the NH closer to the equator. **?** reported that anomalies of These maps visually confirm the linkage between the ITCZ's convective activity and enhanced stratospheric GW Epand OLR from their zonal averages imply that negative (positive) values of Ep and OLR reflect a reduction (increase) or increase (decrease) of GW energy and convection, respectively, and discovered significant relationships between GW activity and OLR measurements (**?**) , while also hinting at complexities beyond a simple one-to-one mapping.

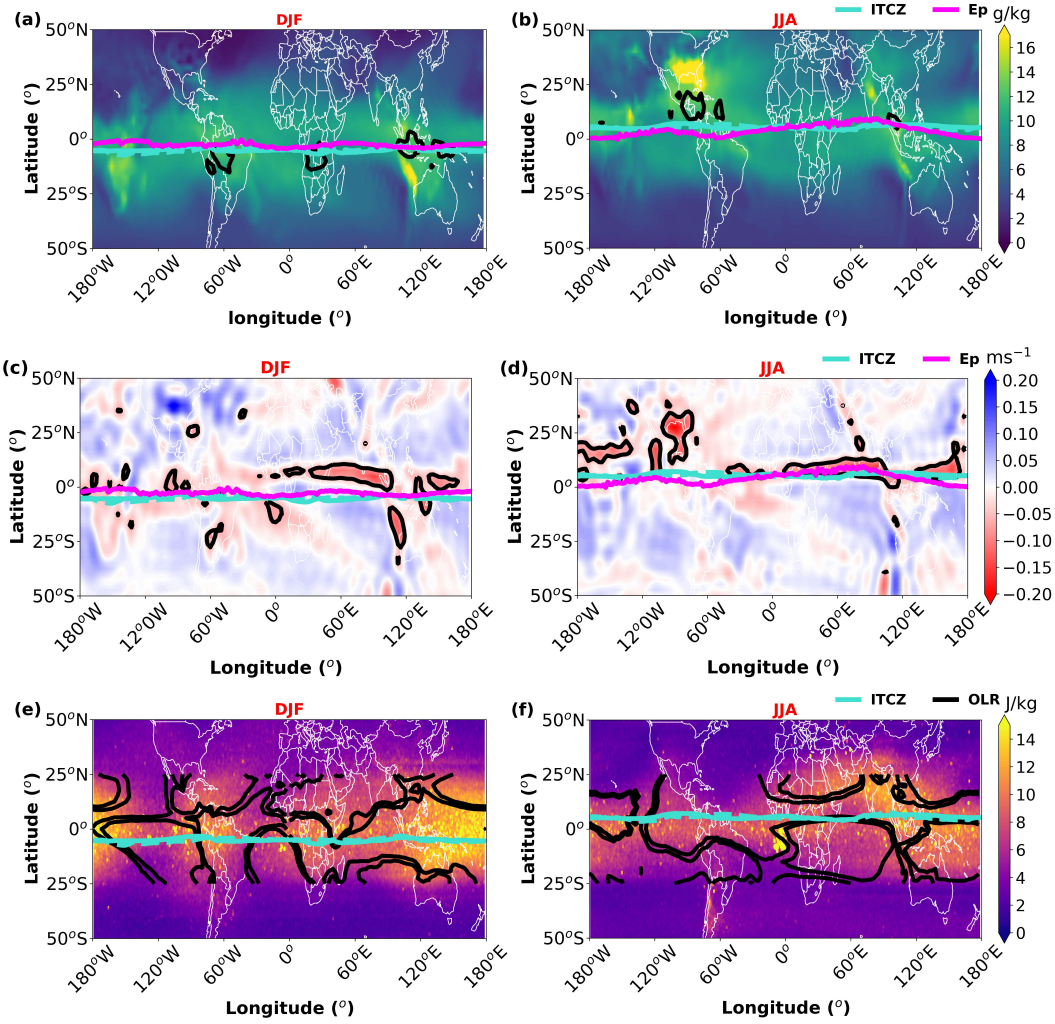

Figure 7. Mean fields (2011-2021) for DJF (left column: **a, c, e**) and JJA (right column: **b, d, f**). Cyan solid line: mean ITCZ location (from RO refractivity at 850 hPa). Magenta solid line: mean Ep maximum location (from RO Ep at 20 km). **(a, b)** Mean specific humidity ($g\,kg^{-1}$, color shading) at 800 hPa. Black contours show OLR between 200 and 250 $W\,m^{-2}$. **(c, d)** Mean vertical velocity (ω, $Pa\,s^{-1}$, negative values indicate ascent; color shading) at 800 hPa. Black contour is the zero vertical velocity line. **(e, f)** Mean Ep ($J\,kg^{-1}$, color shading) at 20 km. Black contours show OLR (200-250 $W\,m^{-2}$).

3.2 ~~Modes of climate variability~~ Interannual Variability and ~~ITCZ and Ep trends~~Longitudinal Structure of Trends

~~In this section, we presented the zonal trends of the 11-year ITCZ derived from RO, ERA5, and NCEP refractivity and the GWs Ep in a and b, also the zonal correlation coefficients between the ITCZ and the Ep in c. presented the relationships between the various atmospheric oscillations (ENSO, MJO, and QBO) and the ITCZ derived from RO, ERA5, NCEP refractivity, and Ep maxima latitudinal locations . depicts the zonal refractivity and Ep values at the Gaussian peak. We also presented in the zonal~~

trends refractivity from RO, ERA5, and NCEP and the Ep values at their Gaussian peak in a and b, and the zonal correlation coefficients between the refractivity and the Ep values in b. presented the relationships between the atmospheric oscillations and the refractivity from RO, ERA5, NCEP, and Ep values.

3.2.1 *ITCZ and Ep maxima location Trends*

The trends of the ITCZ derived from RO, ERA5, and NCEP refractivity and maximum Ep latitudinal locations are shown in . The ITCZ in a showed different positive trends (~0.005-0.011 N/month) at different zonal locations. The trends exhibit variation across the longitudinal sectors. The American sector (~120°W to 60°W) displays generally constant patterns throughout the datasets. Still, Beyond the seasonal cycle, we investigate the interannual variability and long-term trends in the African sector (~60°Wto 60°E)diverges, with a significant drop in the trend for ERA5. Asian sector (~60°E to 120°E) trends are consistent across datasets, with a modest rise reported. Unlike ITCZ trends, the maximum ITCZ and Ep position exhibits a unique oscillation pattern over longitudes b. The trends are typically positive in maxima locations and their peak values over the 11-year period. Figure 8 (top panels) shows the year-to-year variations in the African (~0.006peak locations for DJF and JJA. The ITCZ location (Figure 8a) exhibits interannual shifts of approximately 5°-0.014 J kg^{-1} per month) and Asian sectors (~0.001-0.009 J kg^{-1} per month) but turn negative in the American sector (~−0.004 J kg^{-1} per month) around 60°W and at eastern Pacific. The negative trend in the Ep over the stratosphere in the American sector has earlier been reported by **?**. The transitions between positive and negative trends demonstrate how 15° north and south during the 11-year period, but the overall seasonal migration pattern remains dominant. The Ep latitudinal movements may be affected by regional differences. The zonal coefficients that relate the ITCZ , as determined by ROmaximum location (Figure 8b) shows similar interannual variability, generally tracking the ITCZ shifts but sometimes exhibiting independent variations, especially noticeable over the Pacific Ocean (120°E-120°W), ERA5, and NCEPrefractivity, with Ep maxima latitudinal locations show how strongly the ITCZ corresponds with shifts in Ep locations (c). The coefficients are often larger in the African and Asian sectors, indicating a stronger link between ITCZ and Ep in these regions than in the American sector. The zonal correlation between ITCZ and the GW energy is generally positive, with a correlation above 60% over the Asian monsoon areas. As expected, it showed that most GW activity is generated by mesoscale convective systems in this region (**?**). The low correlations between eastern South America and the western Pacific are a subject of interest, and they could result from associated atmospheric oscillation that influences both ITCZ and the GWs. which is strongly influenced by ENSO.

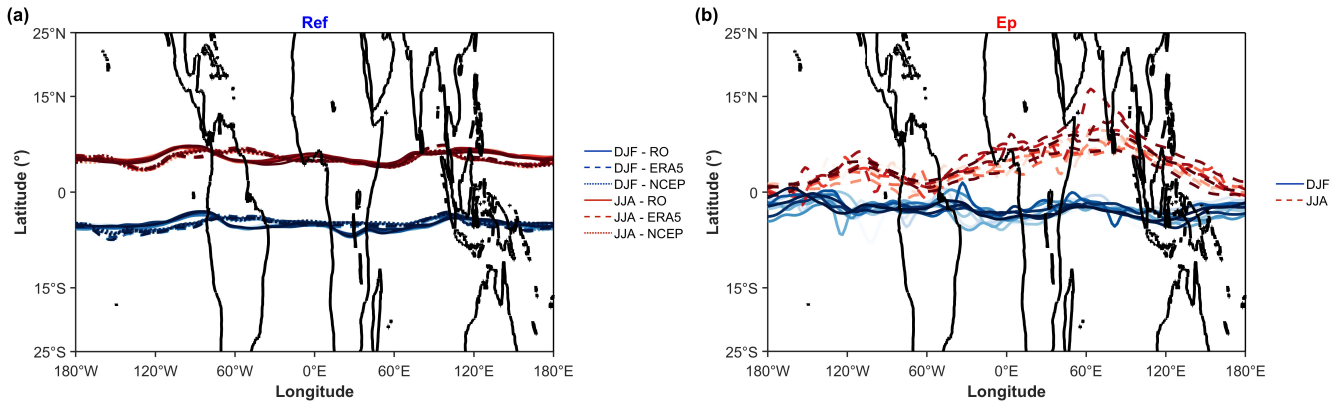

~~The zonal trends and ITCZ coefficients derived from RO, ERA5, NCEP refractivity, and maximum Ep latitudinal locations over 11 years. **(a)** The zonal trends ITCZ derived from RO, ERA5, and NCEP refractivity. **(b)** The zonal trends of the maximum Ep latitudinal location. **(c)** The zonal coefficients of the ITCZ derived from RO, ERA5, NCEP refractivity, and maximum Ep latitudinal locations. The shaded areas mark the American (100°W-30°W), African (10°W-50°E), and Asian sector (100°E-150°E) sectors are marked with shaded regions. The black horizontal dotted lines are the zero demarcation lines.~~

Figure 8. Longitudinal variation of the latitudinal location (ϕ_{max}) of maxima derived from Gaussian fits, showing interannual variability from 2011 to 2021. **(a)** Interannual variability of ITCZ locations for DJF (blue lines) and JJA (purple lines) derived from RO (solid), ERA5 (dashed), and NCEP (dotted) data for each year. **(b)** Interannual variability of Ep maxima locations (from RO) for DJF and JJA (multi-colored solid lines for individual years), compared with the 11-year mean ITCZ locations for DJF (blue dashed) and JJA (purple dashed) for reference.

3.2.1 ~~*Modes of climate variability and ITCZ and Ep maxima locations*~~

~~a depicts zonal regressions of the maximum GW~~ To quantify linear changes over the 11-year period, we applied the multilinear regression method described in Section 2.5 to calculate the trend coefficient (α_0) for the latitudinal position (ϕ_{max}) of the ITCZ and Ep ~~latitudinal locations that include three atmospheric oscillations: ENSO, MJO, and QBO at different pressure levels (30 and 50 mbar, respectively) . The regression coefficients between the maximum Ep latitudinal position and the ENSO coefficients shown in a vary longitudinally, with positive values (0.7 J kg^{-1} per month) in~~ maxima at each longitude (Figure 9). The longitudinal variation of the ITCZ position trend (Figure 9a) fluctuates around zero for RO, ERA5 and NCEP, suggesting no globally coherent, statistically significant linear trend in the ~~Asian sectors but negative values (−0.3 J kg^{-1} per month) in the~~ mean ITCZ latitude over this specific period of 11 years. Trends vary across different longitudinal sectors, with generally positive values (0.060-0.130 degrees latitude per year) indicating a northward shift of the ITCZ over the 11-year period in some regions. Some regional variations exist, with slight positive (northward) tendencies in parts of the American sector and ~~near zero in the African sector. The maximum~~ slight negative (southward) tendencies over parts of Africa in the ERA5 data, but confidence intervals are wide.

The longitudinal variation of the Ep ~~latitudinal position advances northward during positive ENSO phases (El Niño) in the Asian sectors but somewhat southward in America and Africa. The variation across longitudes indicates regional variances in how ENSO affects GW activity (**???**). The regression coefficients between the highest Ep latitudinal location and the MJO are shown in the b. The MJO coefficients are consistently negative (~~maximum position trend (Figure 9b) also shows fluctuations around zero, although with a tendency towards positive trends in the African (~~-0.5--3 J kg^{-1} per month) across all sectors, with larger amplitude in African~~ 0.072-0.170 degrees latitude per year) and Asian sectors ~~. This shows that during active MJO periods, the maximum Ep latitudinal location shifts southward, with a more significant effect in the Eastern Hemisphere. The MJO's consistent negative trend suggests that it has a more uniform influence on GW activityacross longitudes than ENSO. The regression coefficients for the most significant Ep latitudinal location and the QBO at 30 and 50 mbar are shown in a. The coefficients at both pressure levels exhibit similar longitudinal~~ (~0.012-0.010 degrees latitude per year), indicating a northward shift of GW activity. However, negative trends (~~-0.095-0.008 J kg^{-1} per month) but differ in magnitude. In~~ -0.048 degrees latitude per year) are observed in the American sector ~~, the QBO coefficients are around zero or slightly positive (~0.008 J kg^{-1} per month), suggesting minimal influence. However, in the African and Asian sectors, the coefficients turn negative,~~ around 60°W and in the eastern Pacific, suggesting a southward shift ~~in the maximum~~ of GW activity in these regions. This regional variability in Ep ~~latitudinal location during the QBO's westerly phase. The higher values at 50 mbar indicate that the lower stratosphere has a more considerable effect on GW activity than the upper stratosphere (30 mbar). The findings imply that ENSO, MJO, and QBO all play different roles in the zonal variability of localized region GW Ep concentrations, with each oscillation having a more significant impact on specific sectors.~~ trends may reflect differences in how climate variability modes affect GW generation and propagation in different geographical areas. However, these trends are generally not statistically significant in large longitudinal bands within the 11-year record.

~~The zonal regressions of the atmospheric oscillations with the ITCZ derived from RO, ERA5, NCEP refractivity, and maximum Ep latitudinal locations over 11 years. **(a-c)** The zonal regressions of the maximum Ep latitudinal locations with ENSO (**a**, in red lines), MJO (**b**, in blue lines), and QBO at 30 mbar (**c**, orange lines) and at 50mbar (**c**, green lines). **(d-f)** The zonal ITCZ derived from refractivity measurements by RO (solid lines), ERA5 (dashed lines), and NCEP (dotted lines) for ENSO (**d**, in red lines), MJO (**e**, in blue lines), and QBO at 30 mbar (**f**, orange lines) and 50 mbar (**f**, green lines). The shaded areas mark the American (100°W-30°W), African (10°W-50°E), and Asian sector (100°E-150°E) sectors are marked with shaded regions. The black horizontal dotted lines are the zero demarcation lines.~~

~~In d, the regressions show a clear latitudinal shift in the ITCZ due to ENSO. All three datasets exhibit quite similar patterns, with slight variations. There is a positive trend in the American sector, while the trends are negative in~~ Figure 9c shows the correlation coefficient between the monthly time series of the ITCZ position ($\phi_{max,N}$) and the ~~African and Asian sectors. The ERA5 and NCEP exhibit more volatility than the RO, notably in the~~ Ep position ($\phi_{max,Ep}$) at each longitude. Positive correlations dominate globally, with particularly strong values in the African and ~~Asian sectors, indicating model dependency in the response to ENSO. Over the Atlantic Ocean, the~~ Asian sectors (up to ~0.60), indicating that interannual shifts in the ITCZ location are often mirrored by shifts in the stratospheric maximum Ep~~trends continue to show a negative trend, though less pronounced than the Pacific. The Atlantic's influence on global weather patterns, such as the Atlantic Meridional Overturning~~

Circulation (AMOC) (?????), can contribute to these trends. Around the Indian Ocean, . The correlation is particularly strong (above 0.60) in the Ep trends remain negative but with smaller amplitudes, likely due to monsoon and other regional atmospheric processes. The AMOC is a major cycle that transports warm surface water from the tropics and subtropics in the north to the North Atlantic. The increase in the datasets suggests that this relationship is strong and may be influenced by Asian monsoon region, which is consistent with the prevalence of mesoscale convective systems that are a significant source of gravity waves (GWs) (**?**). In contrast, correlations are markedly weaker over the eastern Pacific and Atlantic Oceans. This is physically consistent with the climatological conditions in these areas, particularly the eastern Pacific, which is known as a region of large-scale ocean-atmosphere interactions such as ENSO. Over the Atlantic Ocean, the coefficients are close to zero, indicating a weaker or more complex relationship between refractivity and Ep. The variation may be due to the role of the Atlantic in climate variability, which can produce heterogeneous climates that are not entirely captured by a single parameter. Measurements in the Indian Ocean show a slight positive trend, albeit with some variability. This suggests a downward correlation between refractivity and Ep, possibly influenced by complex interactions of the region with the monsoonal system and the Indian Ocean Dipole (IOD). The IOD is an 'ENSO'-like phenomenon in the Indian Ocean. ENSO is characterized by anomalous warming (El Niño) or cooling (La Niña) over the equatorial Pacific Ocean, peaking in December (**???**). Consistent trends in Ep, especially in the America and over the oceans, indicate a significant decrease in atmospheric energy availability, possibly with global climate events such as ENSO, AMOC, and IOD. The relationship between refractivity and Ep varies, with the American part having a stronger relationship and the African and Asian parts having a more complicated relationship.

The MJO (e) has an apparent adverse effect on the ITCZ across the whole longitudes, especially in Africa, where all datasets indicate substantial decreases. In return, atmospheric subsidence due to the descending branch of the Walker Circulation. This downwelling suppresses the deep convection necessary for strong GW generation. Therefore, even when the ITCZ is present, the African sector receives the most substantial negative response, where all the datasets agree, indicating the connection between MJO and the ITCZ movement. This result also suggests that the influence of MJO does not only affect equatorial stratospheric GW but also atmospheric refractivity. The MJO is relative lack of powerful convective sources weakens the coupling between its position and the primary factor influencing the variability in resulting stratospheric GW activity. The lower correlations observed from eastern South America to the tropical atmosphere for 30 to 90 days. It interacts frequently with the ocean beneath and impacts several weather and climate systems (**?**). The phenomenon involves extensive interconnected patterns of air circulation and convection that move eastward across the Indian and Pacificoceans. MJO is a weather pattern in the lower part of the Earth's atmosphere that features eastward-moving intense thunderstorms and interconnected air movements. Tropospheric convection and wind circulations linked to the MJO influence the propagation of GWs (**?**) and other atmospheric constituents (**?**). A similar result has also been found in Figure 1a of **?**, using the temperature variance to identify the statistical structure of small-scale GWs. Also, large-scale circulations such as the MJO affect the diurnal precipitation cycle, affecting the ITCZ (**?**). The **?** study presents the first observational evidence that the MJO strongly influences the worldwide variability of stratospheric GWs in the tropics.

The QBO (d) impact, most notably at 50 mbar, shows minor but consistent negative trends across all longitudes. The trends at 30 mbar differ considerably amongst datasets, suggesting a greater sensitivity to the dataset used. Both levels (30 western

Pacific may also be related to the influence of climate variability modes that modulate both the ITCZ and ~~50 mbar) exhibited the most significant influence in Africa, with only minor differences between datasets. The ITCZ appears less vulnerable to QBO than ENSO and MJO; however, the patterns are still visible. The RO is substantially consistent with the ERA5 and NCEP, with minor changes. The ERA5 and NCEP data are typically more variable, indicating model or observational changes. The African sector appears particularly vulnerable to all three oscillations, with the most significant changes reported in response to ENSO, MJO, and QBO. The American and Asian sectors reacted quite mildly. These findings emphasize the role of atmospheric oscillations in relocating the ITCZ , with ENSO and MJO having the most significant effect. The QBO also contributes but with less obvious results. Specific trends are similar across datasets, lending legitimacy to observed patterns; nonetheless, regional and model-based discrepancies highlight areas for further exploration~~regional GW activity.

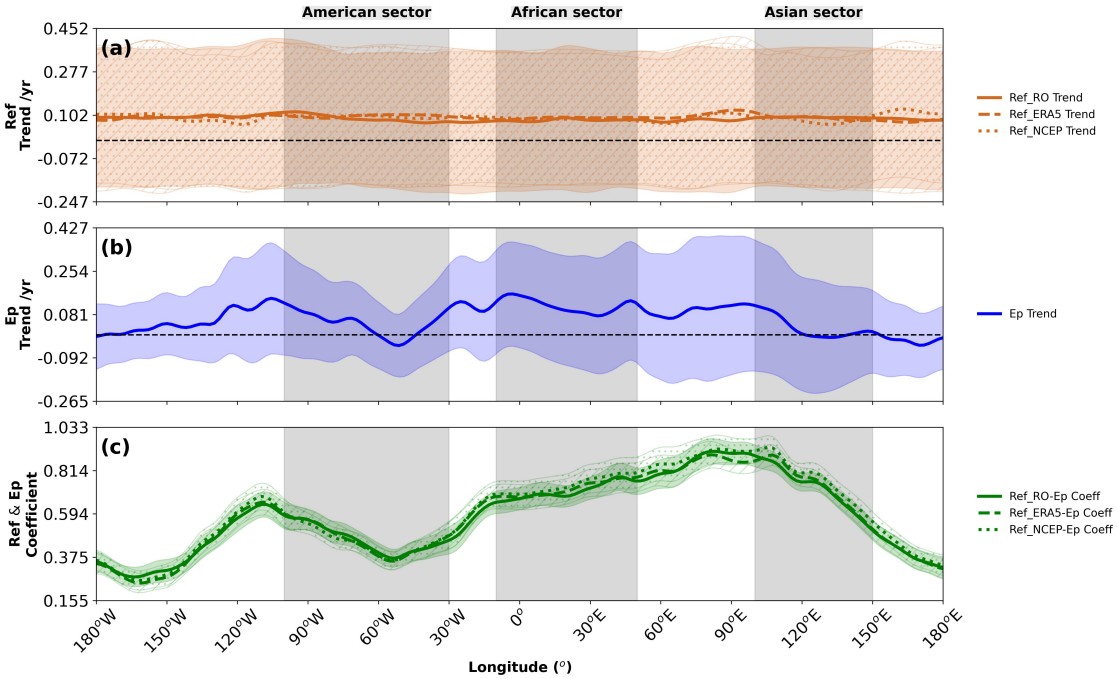

Figure 9. Longitudinal structure of linear trends and correlations for ITCZ and Ep maximum latitudinal locations (ϕ_{max}) over 2011-2021. **(a)** Linear trend in ITCZ latitude (degrees/year) derived from RO (solid red), ERA5 (dashed red), and NCEP (dotted red) refractivity. **(b)** Linear trend in Ep maximum latitude (degrees/year) derived from RO (solid blue). **(c)** Correlation coefficient between monthly ITCZ latitude (RO: solid green; ERA5: dashed green; NCEP: dotted green) and monthly Ep maximum latitude (RO). Vertical shaded regions highlight American (100°W-30°W), African (10°W-50°E), and Asian (100°E-150°E) sectors. Black dashed line indicates zero. Shaded areas are 95% confidence intervals.

3.3 ~~Refractivity and Ep maximum values~~

~~To investigate the relationship between refractivity and Ep, we identified the local maxima of zonal~~ Next, we examine the trends in the peak values (Q_{peak}) of refractivity and Ep ~~at each Gaussian peak, which correspond to the prominent features in the fitted Gaussian profiles, as shown in a,b,c and b. illustrates the zonal refractivity and Ep maxima values at these Gaussian peaks for DJF and JJA (a) and for SON and MAM (b) . We note that MAM signifies the transitional months between DJF and~~ obtained from Gaussian fits. Figure 10 shows the 11-year seasonal mean zonal profiles of these peak values. The peak refractivity values (Figure 10b) show pronounced longitudinal variations, with the highest values over the western Pacific, the Maritime continent and South Asia during JJA, and ~~SON signifies the transitional months between JJA and DJF~~over the Amazon, central Africa and the western Pacific during DJF. These patterns reflect the regions of the most intense convection and convergence. The JJA values are generally higher than the DJF values, particularly in the Asian monsoon region (60°E-120°E), indicating stronger convergence during the summer of the Northern Hemisphere. The American sector shows higher refractivity values during JJA for all datasets, likely due to stronger winds in this region. ~~To further capture the linearity between the two parameters (refractivity and Ep), we further normalized the zonal refractivity and the Ep maxima values at the Gaussian peaks from the result shown in c and d. The refractivity at different seasons seemed to follow the same trend, especially in the transitional months (). The equatorial stratospheric GW Ep during DJF and JJA (a) interchange at different locations, while during SON and MAM (b), the Ep follow the same trend. The results are more apparent for comparison in c and d. Both the refractivity and the Ep at different seasons follow respective trends. We observed an opposite trend between the refractivity and the Ep (increase in refractivity and decrease in Ep) during JJA around 60°W (-60 in c) over tropical South America. The depression in the GW energy over this regioncould be due to JJA tropical dynamics (ENSO, for example).~~

~~During JJA, refractivity values in the American sector peak for reanalysis (ERA5, NCEP) and RO data. The African sector experiences fewer refractivity swings than the American sector, with minor seasonal variations. The Asian sector has occasional peaks, particularly in JJA and MAM, although the shifts are less severe than in the American sector. The most significant increase in the American sector, notably in RO and NCEP data, occurs during the JJA. DJF showed lower refractivity values throughout all sectors. MAM and SON depicted minimal refractivity, with MAM slightly increasing in Asia.~~ The peak Ep values (Figure 10a) also show significant longitudinal variations, but with patterns that do not always match those of refractivity. The highest Ep values occur over the western Pacific and the Maritime continent in both seasons, with secondary maxima over the Amazon and central Africa. Unlike refractivity, the DJF Ep values are generally higher than the JJA values in the ~~American sector drop at around 120°W and 30°W, particularly throughout the DJF, SON, and MAM months. The African sector shows growing~~ western hemisphere (120°W-0°), while the opposite is true in the eastern hemisphere (0°-120°E). This seasonal asymmetry may reflect differences in the efficiency of GW generation, propagation conditions, or the influence of other GW sources. Higher Ep ~~values as it advances eastward, with maximums in the DJF and MAM. The Asian area receives significant increases in Ep, especially between DJF and MAM, indicating higher GW energy. DJF has the highest Ep values in Asia, showing that GW activity is intense throughout the season. While JJA brings lower Ep~~ values ~~, particularly in the American sector. SON Ep values were low, with advances in the African sector, but MAM had considerable increases in both the African~~ in the African and Asian sectors ~~. The American sector has higher refractivity values during JJA, probably due to stronger winds, which coincide with this region's more significant seasonal differences. During~~ during DJF and MAM ~~, the African and~~

~~Asian sectors have higher Ep values, possibly due to more significant~~ may be related to increased convective activity in these regions, ~~resulting in higher GW generation~~ leading to enhanced generation of GW.

The interannual variability, indicated by the shaded areas (one standard deviation), is substantial for both variables, particularly in regions strongly affected by ENSO (120°E-120°W). This variability motivates our regression analysis to quantify the influence of climate modes. ~~The differences in refractivity across the RO, ERA5, and NCEP data indicate that these datasets characterize atmospheric parameters differently, especially in areas of high seasonal variability , such as the American sector.~~

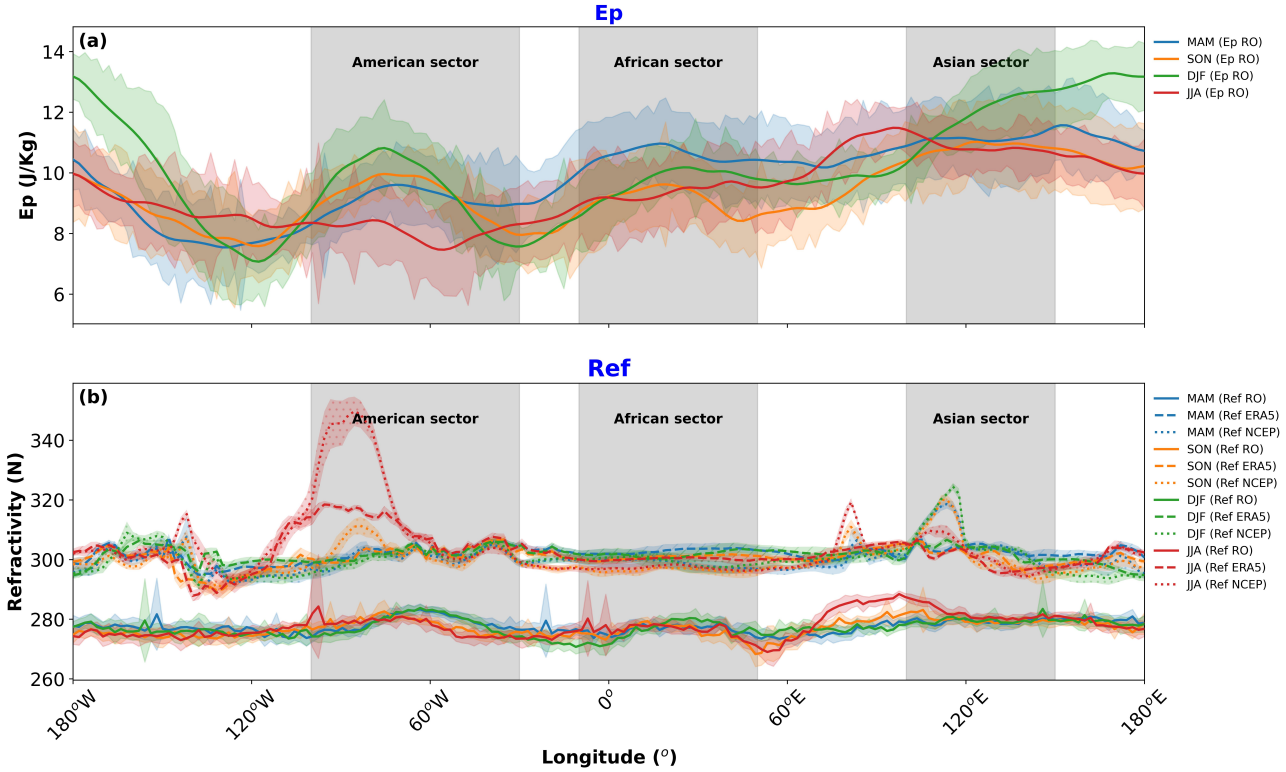

Figure 10. ~~The zonal refractivity from RO (solid line), ERA5 (dashed line), NCEP (dotted line), and Ep~~ Longitudinal profiles of 11-year seasonal mean peak values ~~at their respective maximum~~ derived from Gaussian fits. **(a)** ~~The refractivity values at the~~ Seasonal mean Ep peak ~~of the Gaussian~~ values ($Q_{peak,Ep}$, J kg^{-1}) from RO for DJF (green), MAM (blue), JJA (red), and SON (orange). **(b)** ~~The Ep maxima values are at the~~ Seasonal mean refractivity peak ~~of the Gaussian~~ values ($Q_{peak,N}$, N-units) from RO (solid lines), ERA5 (dashed lines), and NCEP (dotted lines) for DJF (green), MAM (blue), JJA (red), and SON (orange). ~~The shaded areas mark~~ Shading represents the ~~American (100° W-30°W), African (10°W-50°E), and Asian sector (100°E-150°E) sectors are marked~~ standard deviation associated with ~~shaded regions~~the seasonal mean values.

3.2.1 ~~*Trends of refractivity and maximum Ep values*~~

examines the zonal trends and coefficients of Ep and refractivity values at their Gaussian peak in various longitudinal sectors (America, Africa, Asia) and oceans (Pacific, Atlantic, India) using RO, ERA5, and NCEP data. The trends in refractivity vary spatially but generally fluctuate around zero (a) . A The linear trends in these peak values are shown in Figure 11. The trend in peak refractivity (Figure 11a) fluctuates near zero in most longitudes for all datasets, indicating that there is no significant trend in the intensity of the ITCZ peak during this period. The American sector exhibits a slight positive trend is observed for RO and ERA5in the American sector, with , with more significant variations in NCEP. NCEP The African sector shows a slight positive trend for NCEP, while RO and ERA5 remain near zeroover the African sector. Over the ocean, the separation is relatively small , very oceans, the trends are relatively small and stable in the Pacific and Atlantic Oceans, and highly but more variable in the Indian Ocean, which could be influenced by possibly due to regional factors such as precipitation . The trend of patterns.

In contrast, the trend at the peak Ep exhibits a consistently negative pattern b. Over the Pacific Ocean, a similar slightly (Figure 11b) exhibits a predominantly negative trend at most longitudes, suggesting a potential decrease in stratospheric GW activity at the peak over 2011-2021, although the trend is weak and the confidence intervals often overlap zero. The negative trend is observed, associated with broad-scale weather patterns such as ENSO. In c, the American region's relationship between Ep and refractivity values is positive. In contrast, the particularly pronounced in the African and Asian sectors, indicating a more significant reduction in GW activity in these regions. This general decrease in GW activity over the 11-year period may be related to changes in convective activity or background atmospheric conditions.

The correlation between monthly peak refractivity and peak Ep values (Figure 11c) is generally positive, particularly over the American sector and parts of the Pacific, suggesting that stronger ITCZ peaks are often associated with higher stratospheric GW activity. However, the correlation is weaker or more variable in the African and Asian regions show significant changes, making the relationship less clear. Over sectors. In the Pacific Ocean, the coefficients are generally positive, indicating positive correlations, likely probably influenced by large-scale ocean-atmosphere interactions such as ENSO. In contrast, the effects over the Atlantic are The Atlantic Ocean shows coefficients close to zero, indicating a weak correlation. At the same time, , while the Indian Ocean exhibits a positive downward correlationwith some variability, which is likely regionally driven in the atmosphereBut variable correlation.

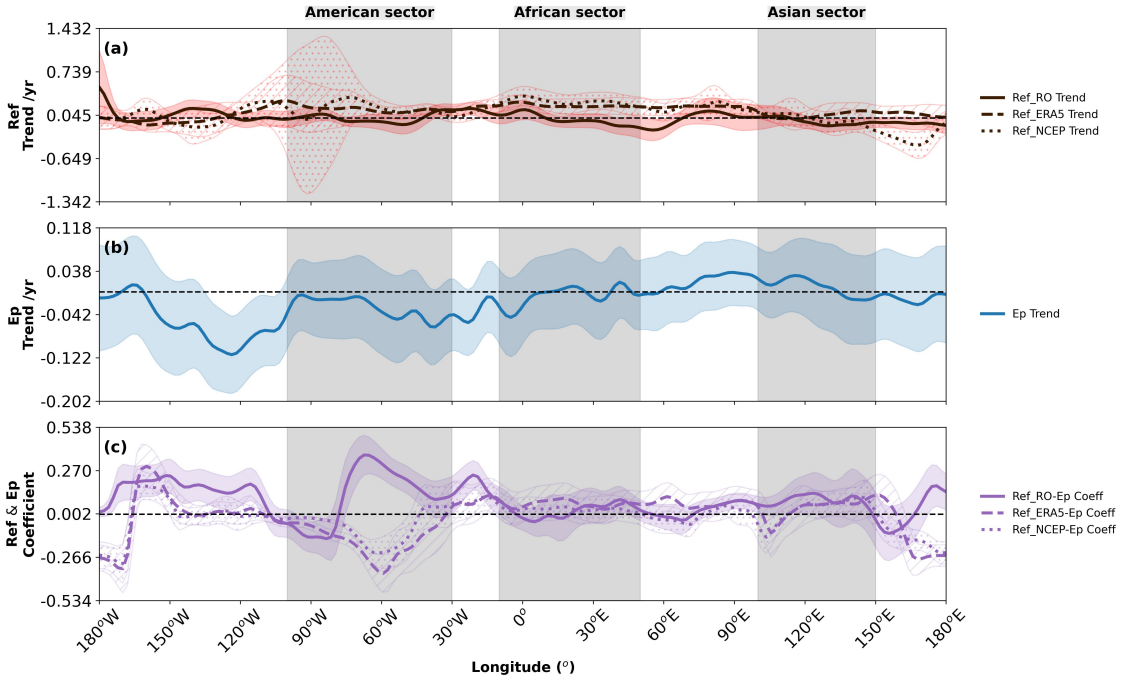

Figure 11. ~~The zonal~~ Longitudinal structure of linear trends and ~~coefficients of the Ep and~~ correlations for ITCZ refractivity ~~from RO, ERA5,~~ peak values ($Q_{peak,N}$) and ~~NCEP at their respective Gaussian~~ Ep peak values ($Q_{peak,Ep}$) over ~~11 years~~2011-2021. **(a)** ~~The zonal trends of~~ Linear trend in peak refractivity (N-units/year) derived from RO (solid ~~line~~red), ERA5 (dashed ~~line~~red), and NCEP (dotted ~~line~~red)~~refractivity Gaussian peak values~~. **(b)** ~~The zonal trends of the Ep Gaussian~~ Linear trend in peak ~~values~~Ep (Jkg^{-1}/year) derived from RO (solid blue). **(c)** ~~The zonal coefficients of the Ep and~~ Correlation coefficient between monthly peak refractivity ~~from~~ (RO~~,~~: solid purple; ERA5~~, and~~: dashed purple; NCEP~~Gaussian peak values. The shaded areas mark the American (100°W-30°W~~: dotted purple) ~~, African (10°W-50°E),~~ and ~~Asian~~ monthly peak Ep (~~100°E-150°E~~RO)~~sectors are marked with~~. Vertical shaded regions ~~. The black horizontal dotted~~ and lines ~~are the zero demarcation lines~~as in Figure 9.

3.2.1 ~~*Modes of climate variability and refractivity and Ep maxima values*~~

~~The zonal trends of Ep and refractivity from the RO, ERA5,~~

3.3 Modulation by Climate Variability Modes

We analyze the regression coefficients (α_1, α_2, α_3 and α_4 in Equation 6) associated to ENSO (MEI.v2), the amplitude of MJO and ~~NCEP Gaussian peak values, each regressed against three significant atmospheric oscillations—ENSO , MJO, and QBO are shown in . The ENSO regression shows positive trends at most longitudes (~~QBO (at 30 hPa and 50 hPa), respectively. Figure 12 shows these coefficients for the latitudinal positions of the ITCZ and Ep maxima.

The ENSO coefficients (Figure 12a, d) show the strongest and most coherent signal among the climate modes. For the ITCZ position (Figure 12a), ~~particularly strong over~~ positive MEI.v2 values (El Niño conditions) are associated with a northward shift in the American sector ~~. The trend increases to the east from 120°W to 90°W longitude, indicating that ENSO influences the area, usually the Pacific. In the~~ (approximately 0.5 degrees latitude per unit ENSO index) and a southward shift in the African and Asian sectors (approximately -0.3 to -0.5 degrees latitude per unit ENSO index). This pattern is consistent across all three datasets, although ERA5 and NCEP show more variability than RO, particularly in the African and Asian ~~regions, the trend slowly decreases but is still positive, which means the effect of ENSO on GW's intensity is consistent. In b, the MJO regression showed alternating oscillations from positive~~ sectors. This pattern reflects the well-known ENSO-induced changes in the Walker circulation, with enhanced convection in the central and eastern Pacific and suppressed convection over the Maritime Continent during El Niño events.

The ENSO influence on Ep maximum position (Figure 12d) shows similar regional patterns, but with some differences in magnitude and spatial structure. The coefficients vary longitudinally, with positive values (up to 0.5 degrees latitude per unit ENSO index) in parts of the Asian sector and negative values (approximately -0.3 to ~~negative. The positive trends are the strongest over the Asian region, specifically for 120°E to 150°E. The trend is less pronounced and variable over the American and African sectors, showing variable influences depending on the region and possibly the phase of the MJO. The MJO also has a significant influence, especially in the Indian Ocean~~ -0.5 degrees latitude per unit ENSO index) in the American sector and parts of the African sector. This indicates that during positive ENSO phases (El Niño), the Ep maxima shift northward in much of the Asian sector but southward in the American sector. These differences may reflect the complex interaction between ENSO-induced changes in convection and stratospheric circulation, which affects GW propagation.

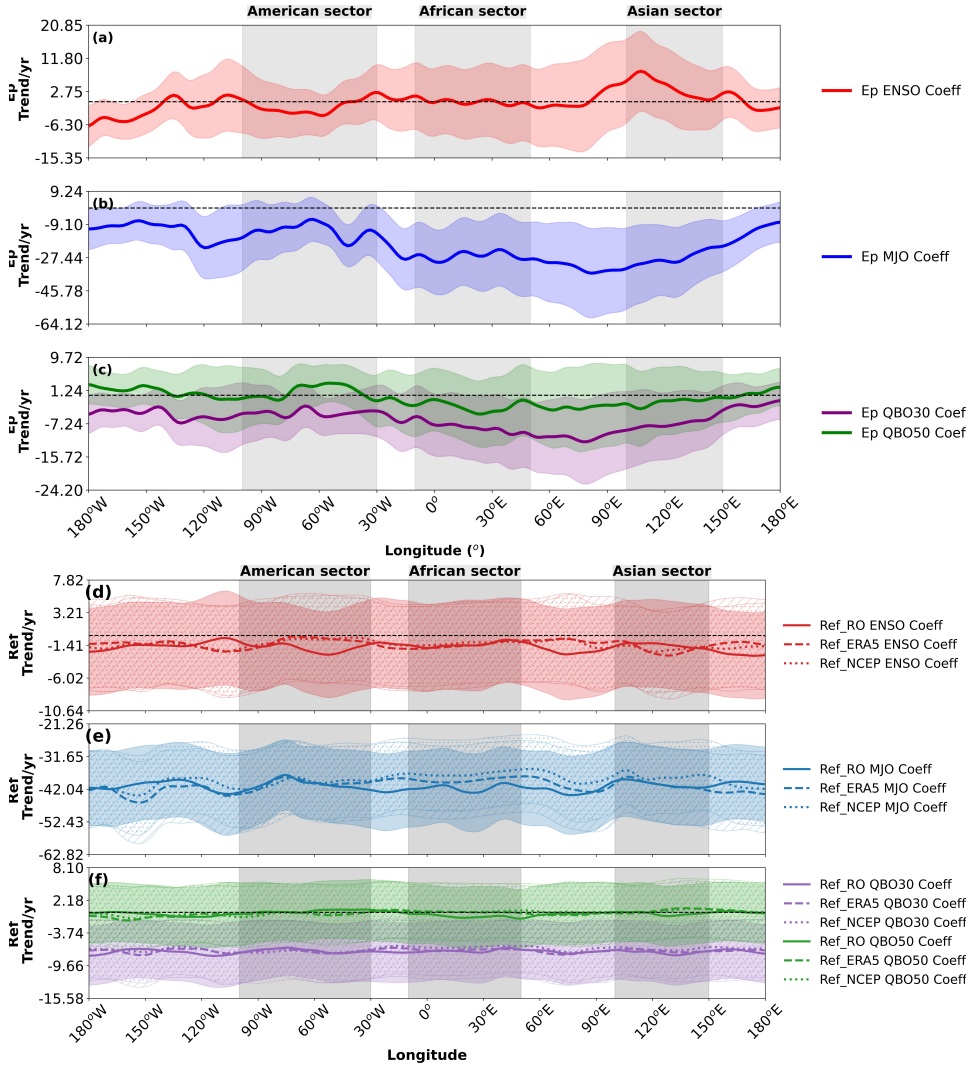

Figure 12. Longitudinal structure of regression coefficients relating climate variability modes to ITCZ and Ep maximum latitudinal positions (ϕ_{max}) over 2011-2021. **(a-c)** Regression coefficients for ITCZ position from RO (solid), ERA5 (dashed), and NCEP (dotted) with **(a)** ENSO (MEI.v2, red), **(b)** MJO amplitude (blue), and **(c)** QBO at 30 hPa (purple) and 50 hPa (green). **(d-f)** Regression coefficients for Ep maximum position with **(d)** ENSO (red), **(e)** MJO amplitude (blue), and **(f)** QBO at 30 hPa (purple) and 50 hPa (green). Units are degrees latitude per index unit. Vertical shaded regions and lines as in Figure 9.

The MJO coefficients (Figure 12b, e) show more localized and generally weaker influences than ENSO. For the ITCZ position (Figure 12b), the MJO coefficients indicate a predominantly negative effect across most longitudes, with the strongest signals in the African and Asian sectors. This suggests that during active MJO periods (higher amplitude), the ITCZ tends to shift southward in these regions by approximately -0.2 to -0.4 degrees latitude per unit MJO index. The pattern shows some

variability across datasets, with RO data exhibiting more pronounced negative coefficients in the African sector compared to reanalysis products. The Maritime Continent and western Pacific ~~region (Asian sector) . The QBO effect is present but more subtle and uneven across sectors. These zonal coefficients highlight the different effects of climate variables on GW dynamics at different latitudes, with ENSO and MJO having the most important effects, especially in the coastal regions where these oscillations are more prominent.~~ (90°E-150°E) show particularly strong MJO effects, where increased MJO amplitude is associated with equatorward shifts. This pattern is consistent with the enhanced equatorial convection during active MJO phases.

~~In c,~~ For the Ep maximum position (Figure 12e), the MJO coefficients show a more complex longitudinal pattern with both positive and negative values. The coefficients are predominantly negative in the African and Asian sectors (approximately -0.2 to -0.4 degrees latitude per unit MJO index), but show more variability in the American sector with some positive values. This suggests that during active MJO periods, the ~~QBO regressions at 30 mbar (QBO30)and~~ Ep maxima generally shift southward in the Eastern Hemisphere but may shift northward in parts of the Western Hemisphere. This regional variation likely reflects the complex interaction between MJO-related convective activity and atmospheric wave dynamics, which can vary significantly with longitude due to differences in land-sea distribution and background atmospheric conditions.

The QBO coefficients (Figure 12c, f) show the weakest influence on the ITCZ position (Figure 12c), which is expected given that QBO is primarily a stratospheric phenomenon. The coefficients show minor but generally negative values across most longitudes, particularly for QBO at 50 ~~mbar (QBO50) showed smaller trends (~ −0.04 to −0.05 J kg^{-1} per month)~~ hPa. The influence is most pronounced in the African sector, with coefficients around -0.1 to -0.2 degrees latitude per unit QBO index, and shows relatively small differences between datasets. This suggests that during the westerly phase of the QBO, the ITCZ tends to shift slightly southward, although the effect is small compared to ENSO and MJO~~, which show more significant effects of the QBO on GW activity. The QBO30 shows slightly negative trends in~~ .

For the Ep maximum position (Figure 12f), the QBO shows a more significant influence, with a distinct longitudinal pattern. The coefficients for both 30 hPa and 50 hPa QBO are near zero or slightly positive in parts of the American sector ~~, while the QBO50 has a more oscillatory structure. Over the Asian sector, especially for 90°E to 120°E longitude degrees , QBO50 exhibits a slightly positive trend, partially indicating an effect in this region. In general, the small magnitudes indicate that although the QBO influences GW strength, the influence is much smaller than that of ENSO and MJO. The most prominent features are related to ENSO , especially in the Pacific region, where the ENSO effect on GW intensity is intense~~but become negative in the African and Asian sectors (approximately -0.1 to -0.3 degrees latitude per unit QBO index). This indicates a southward shift of the Ep maxima during the westerly phase of the QBO in these regions. The QBO at 30 hPa generally shows stronger effects than at 50 hPa, particularly in the Pacific region. This more pronounced effect on Ep compared to the ITCZ reflects the direct influence of QBO on stratospheric wave propagation through critical-level filtering and changes in background wind conditions.

Figure 13 shows the regression coefficients for the peak values of refractivity and Ep with the modes of climate variability. The ENSO coefficients for Ep peak values (Figure 13a) show a distinct longitudinal pattern with predominantly positive values in the American sector (approximately 0.5-1.0 J kg^{-1} per unit ENSO index) and more variable values in the African and Asian

sectors. This indicates that during positive ENSO phases (El Niño), GW activity tends to increase significantly in the American sector and parts of the Pacific region. This enhancement is likely related to increased convective activity during El Niño events, which generates more GWs, particularly in regions where ENSO has a strong influence on tropical convection.

~~The zonal regressions of the atmospheric oscillations with the Ep and refractivity from RO, ERA5, and NCEP at their respective Gaussian peak values over 11 years. **(a-c)** The zonal regressions of the Ep Gaussian peak values with ENSO (**a**, in red line), MJO (**b**, blue line), and QBO at 30 mbar (**c**, orange line) and at 50 mbar (**c**, green lines). **(d-f)** The zonal Refractivity Gaussian peak values by RO (solid lines), ERA5 (dashed lines), and NCEP (dotted lines) regressions with ENSO (**d**, in red lines), MJO (**e**, blue lines), and QBO at 30mbar (**f**, orange line) and 50mbar (**f**, green lines). The shaded areas mark the American (100°W-30°W), African (10°W-50°E), and Asian sector (100°E-150°E) sectors are marked with shaded regions. The black horizontal dotted lines are the zero demarcation lines.~~

~~The correlations of refractivity with ENSO showed significant variability in different longitudes (a)~~For refractivity peak values (Figure 13d), the ENSO coefficients show significant longitudinal variability across all datasets. The RO data (solid red line) ~~implies high positive trends across the globe; it is seen most markedly over the American and Asian sectors, which means the relationship of ENSO with refractivity is rather direct and firm over these~~ shows predominantly positive coefficients across most longitudes, with the strongest signals in the American sector (approximately 2-4 N-units per unit ENSO index) and parts of the ~~globe. The~~ Asian sector. ERA5 and NCEP data ~~(d, dashed and dotted red lines) are also observed to follow the same pattern in general but with slightly less pronounced trends than the RO data. The RO data of the Pacific region (150°W–180° W) and~~ show similar patterns but with some differences in magnitude and regional detail. This suggests a direct relationship between ENSO and refractivity in these regions, with El Niño conditions generally associated with higher refractivity values, indicating enhanced moisture convergence in the lower troposphere.

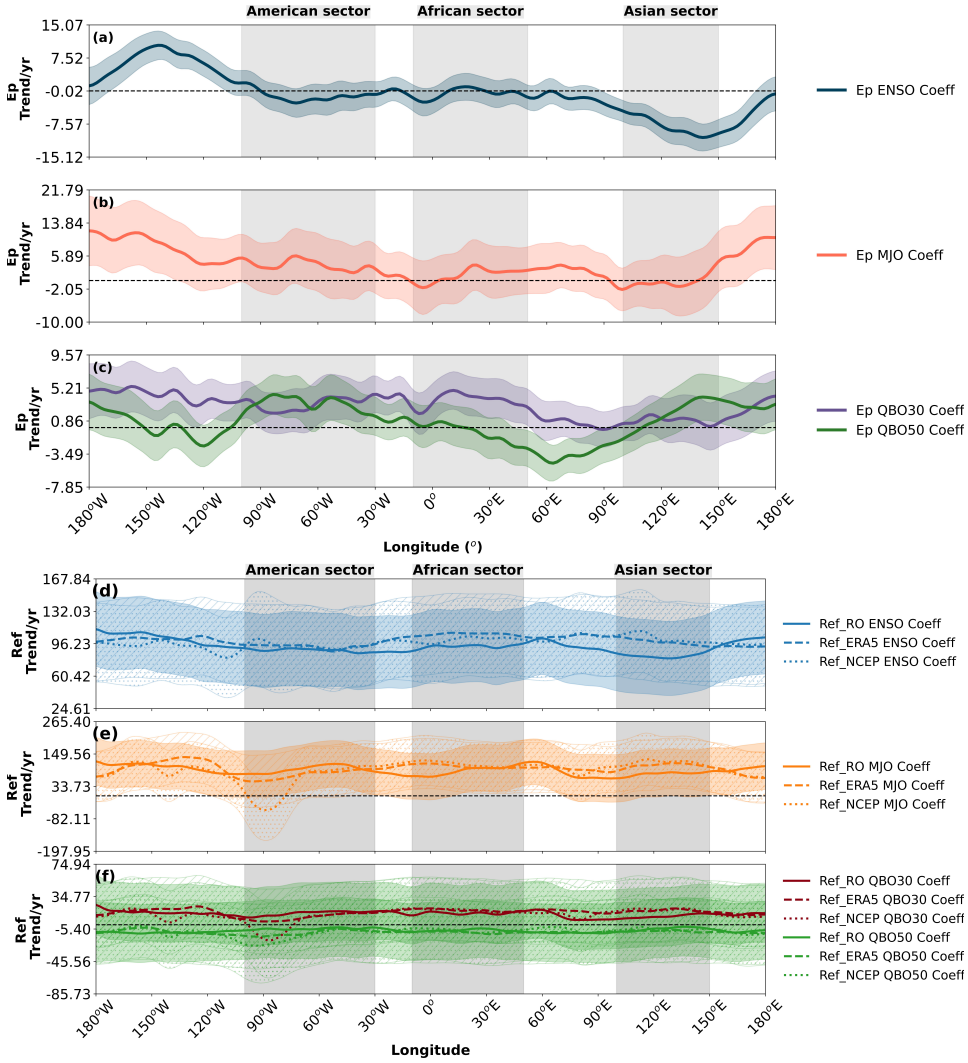

Figure 13. Longitudinal structure of regression coefficients relating climate variability modes to refractivity and Ep peak values (Q_{peak}) over 2011-2021. **(a-c)** Regression coefficients for Ep peak values with **(a)** ENSO (red), **(b)** MJO amplitude (blue), and **(c)** QBO at 30 hPa (purple) and 50 hPa (green). **(d-f)** Regression coefficients for refractivity peak values from RO (solid), ERA5 (dashed), and NCEP (dotted) with **(d)** ENSO (red), **(e)** MJO amplitude (blue), and **(f)** QBO at 30 hPa (purple) and 50 hPa (green). Units are N-units or $\mathrm{J\,kg^{-1}}$ per index unit. Vertical shaded regions and lines as in Figure 9.

The MJO coefficients for the peak values of Ep (Figure 13b) exhibit a complex longitudinal pattern with alternating positive and negative values. Positive coefficients (approximately 0.2-0.5 $\mathrm{J\,kg^{-1}}$ per unit MJO index) are observed in parts of the Asian sector (particularly between 120°E and 150°E) and in limited regions of the American sector, while negative coefficients dominate in the African sector and parts of the Pacific. This pattern suggests that the MJO has a regionally variable influence on

GW activity, likely reflecting the eastward propagation of MJO-related convective anomalies, which enhance GW generation in some regions while suppressing it in others.

For the peak refractivity values (Figure 13e), the ~~Atlantic region (30°W-60°W) show significant positive trends; the RO data is mainly positive. These observations suggest that the influence of ENSO on these sea areas might be more significant, which is connected to the immediate impact of the sea-surface temperature anomalies. The MJO-related refractivity trends (e)were found to have a higher variability among different longitudes, in reckon to ENSO, with the RO data having the most significant change. The trends over the American and Asian regions indicate a high deviation between the RO and reanalysis lines, where the RO trends show~~ MJO coefficients show significant longitudinal variability across all datasets. The RO data (solid blue line) exhibits both positive and negative values~~. The MJO trends~~ , with notable differences from the reanalysis products in some regions. The coefficients are generally negative in the Pacific and Atlantic ~~Oceans result in negative values~~regions, particularly in the NCEP data~~(dotted blue lines), meaning that MJO dampens~~ , suggesting that increased MJO activity tends to reduce refractivity in these ~~regions. The QBO-motivated trends, represented in f as 30 mbar and 50 mbar, point out that QBO has the lowest trend magnitudes over the longitudes (80°W–100°W) , whereas~~ areas. This complex pattern likely reflects the regional variations in how MJO affects tropical convection and moisture distribution, as well as differences in how these processes are represented in observational and reanalysis datasets.

The QBO coefficients for Ep peak values (Figure 13c) are generally smaller in magnitude compared to ENSO and MJO ~~show higher trends. The only consistent trends for the RO, ERA5, and NCEP datasets are their~~ coefficients, indicating a less pronounced but still detectable effect on GW activity. The QBO at 30 hPa (purple line) shows predominantly negative values in the American sector (approximately -0.1 to -0.3 $\mathrm{J\,kg^{-1}}$ per unit QBO index) and more variable values in other regions. The QBO at 50 hPa (green line) exhibits a more oscillatory pattern with alternating positive and negative values across different longitudes, including some positive coefficients in the Asian sector. This longitudinal variability suggests that the QBO's influence on GW activity depends on regional factors such as the background wind structure and the dominant sources of GWs.

For refractivity peak values (Figure 13f), the QBO coefficients have the smallest magnitudes among the three climate modes, consistent with the QBO being primarily a stratospheric phenomenon with limited direct influence on tropospheric processes. The coefficients show slight positive and negative variations around the globe~~. Over the oceans~~, with values generally within ± 1 N-unit per unit QBO index. Over oceanic regions, particularly in the Pacific and Atlantic, most ~~of the trends remain neutral or slightly negative, which means the effect of QBO on the refraction in these areas is almost zero~~QBO trends remain close to zero, indicating minimal effect on lower tropospheric moisture convergence. The small but non-zero coefficients may reflect indirect influences of the QBO on tropospheric circulation through stratosphere-troposphere coupling mechanisms.

~~The~~ These results highlight the different sensitivities of the American, African, and Asian regions ~~show distinct sensitivity~~ to MJO and QBO, ~~and the Americas~~ with the American and Asian regions ~~show~~ showing more pronounced responses to ENSO, especially in the RO data. ~~ENSO effects are most pronounced~~ The effects of ENSO are most significant in oceanic regions, ~~especially in~~ particularly the Pacific Ocean, indicating a strong correlation between sea surface temperature ~~and atmospheric divergence. This finding is consistent with the well-known effects of ENSO on the ocean and atmospheric~~

~~interactions.~~ anomalies and atmospheric refractivity. The MJO shows distinct effects over the ~~ocean, which can produce cold water in some areas,~~ oceans, especially the Pacific~~. The variability could be due to the transient diffusive nature of the MJO phases interacting with oceans (?). On the other hand,~~ , while the QBO exhibits a ~~more negligible~~ smaller effect in oceanic regions~~, suggesting that its effect on refractivity is more pronounced in the troposphere rather than the stratosphere where ocean-atmosphere interactions are stronger.~~ . The RO data often show ~~strong trends , possibly due to~~ stronger trends compared to the reanalysis datasets, possibly because of the higher resolution and sensitivity of the GNSS RO measurements~~compared to reanalysis datasets ERA5. NCEP data typically show weaker trends, possibly due to assimilation of observational data and model constraints.~~ .

In general, our regression analysis demonstrates that climate variability modes significantly modulate both the positions and intensities of the ITCZ and stratospheric GW activity, with distinct regional signatures. ENSO exerts the strongest influence, followed by MJO, while QBO primarily affects the stratospheric GW characteristics rather than the tropospheric ITCZ. These findings highlight the complex interactions between the modes of climate variability and the ITCZ and stratospheric GW activity, with important implications for understanding and predicting tropical atmospheric dynamics.

4 Discussion

~~This study updated the use of RO refractivity data to find the~~

This study investigated the relationship between ITCZ and ~~used COSMIC-2 measurements to show the relationship between the ITCZ and the equatorial stratospheric GW . Refractivity represents the shape of the ITCZ distribution across latitudes and provides a more accurate identification of the ITCZ than other variables, such as precipitation and vertical wind. Therefore, this technique is considered appropriate for the simulated geographic distribution of ITCZs in equatorial stratospheric GW generation. Based on our findings , the equatorial stratospheric GW closely follows the path of~~ stratospheric GW activity in the tropics and how this relationship is modulated by major climate variability modes. Using RO refractivity as a proxy for the ITCZ ~~. Few studies (e.g., **?**, **?**, **?**) have found a good relationship between the features often used as proxies to identify the ITCZ and the equatorial stratospheric GW . For example, **?** found a good correlation between the OLR and equatorial GWs in the lower stratosphere. **?** studied the dynamics of convectively connected GWs traversing the precipitation region using an ideal model for large-scale atmospheric rotation and found that Kelvin waves propagate along the width of the ITCZ in the Rossby radius. Kelvin waves propagate at the speed of the GW ($\sim 15\ \mathrm{ms}^{-1}$), while the propagation speed of a narrow ITCZ is comparable to the speed of a dry GW ($\sim 50\ \mathrm{ms}^{-1}$). **?** confirmed that the propagation characteristics of equatorial trapped Kelvin waves have revealed evidence of convective activity propagating through the central axis of the East Pacific ITCZ.~~

~~The results show that the global ITCZ exhibits a significant and abrupt seasonal movement from DJF to JJA . A thorough analysis reveals that the equatorial jumps of the regional ITCZ over oceanic regions like the Indian Ocean and the western Pacific are the primary cause of~~ and RO temperature profiles to calculate the GW potential energy (Ep), we have demonstrated a clear spatial and temporal correspondence between these phenomena over the 11-year period (2011-2021).

Our analysis confirms that the ITCZ, identified by refractivity measurements, shows a clear seasonal migration between the hemispheres, shifting approximately 10° in latitude between DJF and JJA. This seasonal movement follows the region of maximum solar heating and is consistent with previous studies (**?????**). The stratospheric GW activity, as indicated by the Ep maxima, exhibits similar seasonal patterns but with some notable differences. The latitudinal separation between the DJF and JJA Ep maxima (approximately 5°) is consistently smaller than that of the ~~abrupt migration in JJA. In contrast, contributions from South America and the western and central Pacific are the primary cause of the migration in DJF. In contrast to the **?** results show that there is no dramatic movement of the regional ITCZover Africa, the eastern Pacific, or the Atlantic regions, our results showed a northward shift during JJA/SON and an equatorward shift during DJF/MAM over Africa and the Indian Ocean. This result was also evident in the~~ ITCZ (approximately 10°), suggesting that while the generation of GWs is linked to the ITCZ, their propagation and stratospheric distribution are influenced by additional factors, most notably the filtering effects of the background winds, such as the QBO, Stratospheric Jets, Sudden Stratospheric Warmings (SSWs) etc.

The GW Ep ~~maxima, which showed the most significant seasonal latitudinal difference. As mentioned earlier,~~ maximum is typically located slightly equatorward of the ITCZ, particularly during JJA. This offset probably reflects the influence of stratospheric winds on GW propagation. During JJA, stratospheric easterlies in the summer (Northern) hemisphere tend to filter out eastward-propagating GWs, while allowing westward-propagating waves to reach higher altitudes (**?**). This filtering effect, combined with the meridional propagation of GWs away from their sources, can shift the region of maximum GW activity relative to the convective source region.

The convergence of Ep maxima over the South American Amazon and the equatorial Pacific, where the seasonal positions nearly coincide, is a particularly interesting feature. These regions are characterized by persistent deep convection (**???**) and, in the case of the Pacific, by the presence of a double ITCZ (**???**). The convergence suggests that these areas maintain relatively constant GW activity throughout the year, despite seasonal changes in the ~~ITCZ follows, and the trade winds converge further in the SH, resulting in clouds with deep convective systems that force the ITCZ to move southward. In JJA, the ITCZ returns, and the trade winds concentrate in the NH. Our findings on the location of the ITCZ are consistent with those of previous studies by **????**.~~ ITCZ position.

~~The results in d show a high global variability near the ITCZ and that GW~~ The spatial relationship between ITCZ and GW activity is further supported by the correspondence between regions of high refractivity, low OLR (indicating deep convection), upward vertical motion, and enhanced Ep ~~shows regional differences in climate dynamics. Collecting data to reveal the complexities of these approaches entirely is essential, as evidenced by the different trends and ratios between the datasets. The link between ITCZ activity and GW changes in Africa and Asia could result from significant regional phenomena like deep convective and monsoon activities, as indicated by the significant coefficients in these sectors. Understanding these relationships is essential to our ability to do more in the ITCZ and improve climate conditions. MJO, ENSO, and QBO directly affect the position and strength~~ values. This relationship is particularly strong over land areas, such as South America, Africa, and the Asian monsoon region, where deep convective systems are more intense and frequent. The positive correlation found between ITCZ position shifts and Ep position shifts, and between peak refractivity values and peak Ep values across many

longitudes, reinforces the physical link between ITCZ convective strength/location and the resulting stratospheric GW activity.

However, some discrepancies are observed, particularly over western and equatorial South America during JJA, where GW activity decreases despite the presence of the ITCZ~~(??), and the effects on wind and temperature. The ITCZshifts southward during El Niño events and northward during La Niña (?). These changes in the location of the ITCZ affect the formation and propagation of GWs, which are often initiated by the ITCZ and convective activity . Moreover, the vertical radiation associated with these oscillations may affect the growth and propagation direction of the GW (?????). Understanding these deep interactions is critical for a better understanding of tropospheric and stratospheric two-way interactions~~This suggests that factors other than ITCZ, such as changes in background wind conditions or ENSO-related drying, can modulate GW activity in certain regions and seasons. The complex interplay between convective sources, background atmospheric conditions, and wave propagation processes highlights the need for a comprehensive approach to understanding the generation of GW in the tropics.

~~The ENSO can influence the relationship between the ITCZ and GW through various mechanisms (e.g., Atmospheric Circulation Changes, Ocean-Atmosphere Interaction, Changes in Convection, Wave-Mean Flow Interaction, Stratosphere-Troposphere Coupling). At the time of~~ Our multilinear regression analysis reveals significant influences of climate variability modes on both the ITCZ and stratospheric GW activity, with distinct regional patterns and varying magnitudes of impact. ENSO emerged as the dominant mode of variability. During El Niño ~~occurrences, the Walker circulation—an east-west atmospheric circulation along the equatorial Pacific, characterized by low-level trade winds converging towards the western Pacific and upper-level return flow—weakens. This weakening causes shifts in the position and strength of the ITCZ, leading to changes in precipitation conditions and wind patterns as GW changes (?).~~ conditions, the ITCZ position tends to shift northward in the American sector but southward in the African and Asian sectors. The Ep maximum position under El Niño shifts northward in the Asian sector but southward in the American sector. These patterns are consistent with ENSO's large-scale alterations of tropical circulation (e.g., Walker circulation) and convective centers (???). Furthermore, El Niño ~~events also increase activity , intensifying cloud formation (?). Increased convective activity, specifically the rising motion of warm air masses, contributes to the structure and strength of GWs that affect the ITCZ. According to ?, ENSO-related variations in deep convection are mostly confined north of the equator, a meridional pattern not effectively captured by averages in~~ generally enhances peak GW activity (Ep values), particularly in the American sector and over the Pacific, and also tends to increase peak refractivity values, likely due to intensified or reorganized convection (?). The differences in ENSO's impact on Ep maximum position versus ITCZ position suggest that ENSO affects GW activity not only by modulating convective sources but also by altering stratospheric conditions influencing wave propagation, such as changes in subtropical jets and the Brewer-Dobson circulation (?).

The MJO's influence is characterized by a fairly consistent southward shift of both the ITCZ position and the Ep maximum position during active MJO periods (higher amplitude), with the strongest effects on ITCZ position over the Maritime Continent/western Pacific and for Ep position in the ~~equatorial-centered ENSO region. This imbalance in ENSO atmospheric anomalies is caused by the meridional asymmetry of the eastern Pacific climate, in which the south of the equator is typically below the convection threshold, and the ITCZ is shifted north of the equator (?). According to ?, the MJO might influence stratospheric GWs in~~

two main ways. First, the MJO's convection modulation may affect GW excitation. Second, MJO tropospheric wind anomalies could influence wave propagation African and Asian sectors. The impact of MJO on peak Ep values and peak refractivity values is more variable longitudinally, showing alternating positive and negative regression coefficients. This variability may reflect the eastward propagation of MJO convective anomalies and its complex interaction with background conditions (**???**). The monthly mean data used here might smooth some MJO intraseasonal signals.

The QBO's influence is weaker on the tropospheric ITCZ compared to stratospheric GWs. Westerly QBO phases are associated with small southward shifts in ITCZ position and more noticeable southward shifts in Ep maximum position, particularly in the African and Asian sectors. QBO's impact on peak Ep values and peak refractivity values is generally subtle. This is consistent with QBO primarily modulating GWs through critical-level filtering . Thus, these mechanisms may affect stratospheric GWs and atmospheric refractivity. Few studies have examined how the MJO affects stratospheric GWs. Also, **?** predicted that the lower convection during the MJO's inactive phase would yield higher stratospheric GW energy and momentum fluxes than the active phase because of better vertical propagation of the longer vertical wavelengths.

In this study, we determined the global ITCZ from RO refractivity (COSMIC and METOP satellites) and ERA5 and NCEP reanalysis data, as well as Ep maxima in the equatorial region using the Gaussian fitting method from 2011 to 2021. Using these estimates, we investigated the trends and relationships between the ITCZ and GW Ep maxima locations for variations across different longitudinal sectors and the effects of modes of climate variability such as ENSO, MJO, and QBO. The ITCZ position shifts by about 10° in DJF and JJA and by about 5° in SON and MAM over the ocean regions globally. Generally, altering stratospheric wave propagation conditions rather than directly forcing tropospheric convective strength (**????**).

Regarding long-term trends over 2011-2021, our analysis indicates that the ITCZ latitudinal position shows weak and regionally varying trends, with some tendency towards northward shifts in certain areas, though often not statistically significant over large bands. Similarly, the Ep maximum position trend also fluctuates regionally, with northward tendencies in the African/Asian sectors and southward in parts of the ITCZ derived from RO and reanalysis data shows a similar pattern. The position and strength of American sector, again with wide confidence intervals. These findings are broadly consistent with other studies suggesting complex regional responses rather than a uniform global shift over similar timescales (**?**).

In contrast to the latitudinal positions, trends in the peak values show different behaviors. Peak refractivity values at the ITCZ show little consistent change over the 11-year period, fluctuating near zero across most longitudes. This suggests that while the ITCZ position might undergo subtle shifts, its peak intensity (as measured by refractivity) has remained relatively stable over this period. However, peak Ep values show a predominantly negative trend across most longitudes, indicating a potential general decrease in peak stratospheric GW activity. This decrease is particularly noted in the African and Asian sectors. The contrasting trends between ITCZ peak intensity and GW peak activity suggest that factors beyond just the peak convective strength within the ITCZ, such as changes in the broader convective characteristics, background atmospheric conditions (temperature gradients, wind shears affecting wave generation or propagation), or an increase in wave filtering, might be influencing the observed GW activity. A negative trend in GW activity could have implications for the momentum budget of the middle atmosphere and the ITCZ vary from year to year. The interannual variability has been about ~5° to the north and south. The global equatorial driving of large-scale circulations.

Our study demonstrates the utility of RO data for investigating both tropospheric and stratospheric processes. The high vertical resolution of RO measurements makes them particularly valuable for detecting GWs with short vertical wavelengths, which are often poorly resolved in reanalysis models. The global coverage and all-weather capability of RO observations also provide advantages over other remote sensing techniques, particularly in remote oceanic regions where conventional observations are sparse. The use of refractivity as an ITCZ proxy proved effective, and our refractivity-derived ITCZ positions showed good agreement with traditional indicators such as specific humidity, vertical velocity, and OLR. This approach leverages the sensitivity of RO refractivity to water vapour in the lower troposphere, providing a physically-based method for tracking the ITCZ that is consistent with its definition as a zone of convergence.

5 Conclusions

This study investigated the relationship between the ITCZ and stratospheric GW activity and its modulation by major climate variability modes using GNSS RO data from COSMIC-1, COSMIC-2, and METOP satellites (2011-2021), complemented by ERA5 and NCEP reanalyses. We used refractivity at 850 hPa as an ITCZ proxy and temperature profiles around 20 km for GW potential energy (Ep) calculation, employing Gaussian fitting to identify latitudinal peaks and multivariate regression to quantify climate mode modulation. Our key findings are summarized below:

- The ITCZ and stratospheric GW Ep maxima ~~showed seasonal changes similar to the ITCZ. The global equatorial stratospheric GW~~ exhibit coherent seasonal migrations, shifting approximately 10° in latitude between DJF and JJA, generally following solar heating. The stratospheric Ep ~~maxima were more consistent in the NH and SH and had a much smaller gap than the ITCZ . The~~ maximum is typically located slightly equatorward of the ITCZ, particularly during JJA, with a smaller seasonal latitudinal separation (∼5°) compared to the ITCZ (∼10°), indicating the seasonal correspondence in the concentration of stratospheric GW Ep and the ITCZ.

- A strong spatial relationship exists between the ITCZ and enhanced GW activity, especially over landmasses like South America, Africa, and the Asian monsoon region. This is supported by the alignment of ITCZ and Ep ~~position changes by 5° during DJF, JJA, and between SON and MAM. The Ep maxima in DJF and JJA suggest two sites of convergence over the South American Amazon and the equatorial Pacific. Our results show that the ITCZ positions are consistent with other features such as~~ maxima with high specific humidity, low OLR, and ~~vertical wind data. Our results showed good agreement between OLR and peak-specific humidity, especially at DJF. The refractivity and Ep maxima exhibited opposite trends in certain regions, notably during JJA over tropical South America, where increased refractivity coincided with decreased Ep. The ITCZ derived from RO and reanalysis data shows different patterns in trendsat different longitudinal geolocations and the refractivity values at the peak of the Gaussian. The ITCZ showed positive trends in its latitudinal position, with variability across different longitudinal sectors. The correlation between ITCZ~~ upward vertical motion, confirming deep convection as a primary GW source. Both features display significant

longitudinal variations in their positions, peak values, and trends, reflecting regional geographical and circulation influences.

- ENSO exerts the most substantial modulation on both ITCZ and GW Ep ~~positions was higher~~ characteristics, with distinct regional patterns. El Niño conditions correlate with northward ITCZ shifts in the American sector and southward shifts in the African and Asian sectors~~, indicating a solid link between these parameters. The zonal correlation between ITCZ and GW energy was positive overall, especially~~. For GW Ep maxima, El Niño leads to northward shifts in the Asian ~~monsoon regions, implying that convective systems on a mesoscale level are significant sources of GWs in those regions. The ENSO affected~~ sector but southward shifts in the American sector. ENSO generally enhances GW activity (peak Ep ~~and ITCZ locations differently in different subregions. Positive ENSO phases brought about a north shift of Ep in the Asian sectors and a~~ values) and peak ITCZ refractivity, particularly evident in RO data.

- MJO consistently induces a southward shift of ~~these locations in the American and African sectors. The ITCZ also showed a positive trend in the American sector, while negative trends were revealed~~ both the ITCZ and Ep maxima positions across many longitudes during active phases, with the strongest impact on ITCZ position over the Maritime Continent/western Pacific and on Ep position in the African and Asian sectors. ~~The MJOconsistently negatively influenced the~~ Its influence on GW and refractivity peak values shows zonal variations linked to MJO's eastward propagation.

- QBO shows a weaker but detectable influence, primarily on stratospheric GW Ep~~maxima locations across all sectors, with a southward shift being more pronounced in~~ , with minor effects on the tropospheric ITCZ. Westerly QBO phases are generally associated with southward shifts in Ep maxima, especially in the African and Asian sectors~~. The MJO also strongly impacted the ITCZ, especially in the African sector, indicating a substantial negative influence on atmospheric refractivity and GW activity. The QBO's influence was less relevant than that of the ENSO and MJO, with the QBO showing a negative effect that was consistent across all longitudes, albeit more mild at 50 mbar. The region of Africa showed the most significant sensitivity to QBO, and the ITCZ showed some sensitivity to this oscillation. The variations showed that the refractivity peaked positively in the American sector during JJA.~~ , and subtle changes in wave amplitudes due to altered propagation conditions.

- Over the 2011-2021 period, the ITCZ latitudinal position shows weak and regionally varying trends, while the Ep maxima position also exhibits regional variability without a strong global trend. In contrast, peak refractivity at the ITCZ shows little consistent change, whereas peak Ep ~~values were highest in the African and Asian sectors during DJF and MAM, likely during convective activities that increased. The study reveals the different ENSO, MJO, and QBO modulations on atmospheric refractivity over different longitude sectors and distinct continents. ENSO showed a more significant contribution to ENSO, especially over oceans~~values display a predominantly negative trend across most longitudes, suggesting a potential decrease in peak stratospheric GW activity. Interannual variations in ITCZ and Ep positions and strengths are positively correlated in many regions, further supporting their physical connection.

- RO, ERA5, and NCEP generally agree on the mean ITCZ structure and broad modulation patterns, but RO data often reveal stronger responses and trends, likely due to their higher resolution and direct sensitivity to atmospheric properties, highlighting the value of RO observations for studying atmospheric wave dynamics.

5.1 Limitations

Several limitations of our study should be acknowledged. First, the 11-year period (2011-2021) is relatively short to detect robust climate trends, and observed trends may be influenced by natural variability rather than long-term climate change. Longer time series would provide more confidence in the trend estimates and allow for better separation of different timescales of variability. Second, our analysis focused on monthly mean data, which may smooth out important sub-monthly variations, particularly for phenomena like the MJO. Future studies using higher frequency data could provide more detailed information on the intraseasonal modulation of the ITCZ-GW relationship. Third, while our regression model accounts for the linear influences of climate modes, it does not capture potential nonlinear interactions between different modes or lagged relationships. More sophisticated statistical techniques, such as nonlinear regression or machine learning approaches, could potentially reveal more complex patterns of climate-mode influences. Fourth, our study was limited to a single altitude level (20 km) for GW analysis. Extending the analysis to multiple levels would provide a more complete picture of GW propagation and dissipation throughout the stratosphere and mesosphere. Finally, while our observational approach provides valuable insight into the ITCZ-GW relationship and its modulation by climate modes, it does not directly address the underlying physical mechanisms. Complementary modeling studies, ideally using high-resolution models that can explicitly resolve GWs, would help to elucidate the causal pathways linking climate variability, convection, and wave dynamics.

Data availability. CDAAC, ECMWF, and NOAA exclusively provide the data used in this study, and they were obtained from http://cdaac-www.cosmic.ucar.edu/cdaac, https://www.ecmwf.int/en/forecasts/dataset/ecmwf-reanalysis-v5, https://psl.noaa.gov/data/gridded/data.ncep.reanalysis.html, respectively.

Author contributions. Conceptualisation, Ayorinde, T. T., Wrasse, C. M., and Takahashi, H.; methodology, Ayorinde, T. T.; software, Ayorinde, T. T.; validation, Wrasse, C. M., Takahashi, H., and Sapucci, L. F.; formal analysis, Ayorinde, T. T.; investigation, Ayorinde, T. T.; resources, CDAAC; data curation, Ayorinde, T. T.; writing—original draft preparation, Ayorinde, T. T.; writing—review and editing, Wrasse, C. M., Takahashi, H., Sapucci, L. F., and Figueiredo, C. A. O. B.; visualisation, Barros, D. and Essien, P.; supervision, Wrasse, C. M., and Takahashi, H.; project administration, Ayorinde, T. T.; funding acquisition, Wrasse, C. M.

Competing interests. The authors declare that there are no competing interests.

Acknowledgements. The authors ~~acknowledged~~ acknowledge CDAAC, ECMWF, and NOAA for providing the data. We also acknowledge the financial support provided by the Brazilian Ministry of Science, Technology, and Innovations (MCTI) and the Brazilian Space Agency (AEB) ~~underf~~ under the grant number 20VB.0009 and the Conselho Nacional de Desenvolvimento Científico e Tecnológico (~~CNPQ~~CNPq) under the process ~~number~~ numbers $141373/2019-9$ ~~,~~ and $303871/2023-7$. Thanks to Fundação de Apoio ~~a pesquisa do estado~~ à Pesquisa do Estado da Paraíba (FAPESQ) under the process number $2021/04696-6$ ~~. Thanks~~ and to Fundação de Apoio ~~a pesquisa do estado da Sao~~ à Pesquisa do Estado de São Paulo (FAPESP).